European Journal of Medicinal Chemistry 270 (2024) 116353

Contents lists available at ScienceDirect

European Journal of Medicinal Chemistry

journal homepage: www.elsevier.com/locate/ejmech

Research paper

Novel 6-alkyl-bridged 4-arylalkylpiperazin-1-yl derivatives of azepino [4,3-*b*]indol-1(2*H*)-one as potent BChE-selective inhibitors showing protective effects against neurodegenerative insults

Francesco Samarelli [a,2], Rosa Purgatorio [a,2], Gianfranco Lopopolo [a,1], Caterina Deruvo [a], Marco Catto [a], Michael Andresini [a], Antonio Carrieri [a], Orazio Nicolotti [a], Annalisa De Palma [b], Daniela Valeria Miniero [b], Modesto de Candia [a,*], Cosimo D. Altomare [a]

[a] Department of Pharmacy-Pharmaceutical Sciences, University of Bari Aldo Moro, Via E. Orabona 4, 70125, Bari, Italy
[b] Department of Biosciences, Biotechnologies and Environment, University of Bari Aldo Moro, Via E. Orabona 4, 70125, Bari, Italy

ARTICLE INFO

Keywords:
Azepino[4,3-*b*]indol-1(2*H*)-One
Acetylcholinesterase
Butyrylcholinesterase
Amyloid-β aggregation
Oxidative stress
Glutamate excitotoxicity
Neuroprotection

ABSTRACT

Due to the putative role of butyrylcholinesterase (BChE) in regulation of acetylcholine levels and functions in the late stages of the Alzheimer's disease (AD), the potential of selective inhibitors (BChEIs) has been envisaged as an alternative to administration of acetylcholinesterase inhibitors (AChEIs). Starting from our recent findings, herein the synthesis and *in vitro* evaluation of cholinesterase (ChE) inhibition of a novel series of some twenty 3,4,5,6-tetrahydroazepino[4,3-*b*]indol-1(2*H*)-one derivatives, bearing at the indole nitrogen diverse alkyl-bridged 4-arylalkylpiperazin-1-yl chains, are reported. The length of the spacers, as well as the type of aryl-alkyl group affected the enzyme inhibition potency and BChE/AChE selectivity. Two compounds, namely **14c** (IC_{50} = 163 nM) and **14d** (IC_{50} = 65 nM), bearing at the nitrogen atom in position 6 a *n*-pentyl- or *n*-heptyl-bridged 4-phenethylpiperazin-1-yl chains, respectively, proved to be highly potent mixed-type inhibitors of both equine and human BChE isoforms, showing more than two order magnitude of selectivity over AChE. The study of binding kinetics through surface plasmon resonance (SPR) highlighted differences in their BChE residence times (8 and 47 s for **14c** and **14d**, respectively). Moreover, **14c** and **14d** proved to hit other mechanisms known to trigger neurodegeneration underlying AD and other CNS disorders. Unlike **14c,** compound **14d** proved also capable of inhibiting by more than 60% the *in vitro* self-induced aggregation of neurotoxic amyloid-β (Aβ) peptide at 100 μM concentration. On the other hand, **14c** was slightly better than **14d** in counteracting, at 1 and 10 μM concentration, glutamate excitotoxicity, due to over-excitation of NMDA receptors, and hydrogen peroxide-induced oxidative stress assessed in neuroblastoma cell line SH-SY5Y. This paper is dedicated to Prof. Marcello Ferappi, former dean of the Faculty of Pharmacy of the University of Bari, in the occasion of his 90th birthday.

1. Introduction

Alzheimer's disease (AD) is the age-related neurodegenerative disorder, which accounts for the most widespread dementias in the world. As estimated by the World Alzheimer Report, due to the lack of disease-modifying therapies, the number of AD patients is expected to increase to more than 30 million by 2050 [1–4]. The main histopathological hallmarks characterizing AD are the deposition of senile plaques, containing both extracellular neurotoxic β-amyloid (Aβ) peptide aggregates, intracellular neurofibrillary tangles of hyperphosphorylated τ-protein, and decreased levels of neurotransmitter acetylcholine (ACh) in cholinergic neurons of neocortex, hippocampus, and finally in whole brain, leading to impairment in learning, memory, behavior and emotional responses [5,6].

Decades of research identified main targets involved in physiopathology of AD but, despite the efforts and resources employed, only recently two monoclonal antibodies against amyloid protein (aducanumab and lecanemab), underwent accelerated approval by FDA as

* Corresponding author.
E-mail address: modesto.decandia@uniba.it (M. de Candia).
[1] Present address: Research & Development Department, Newchem SpA, Via Roveggia 47, 37138 Verona, Italy.
[2] Equally contributing authors.

https://doi.org/10.1016/j.ejmech.2024.116353
Received 16 January 2024; Received in revised form 18 March 2024; Accepted 19 March 2024
Available online 20 March 2024

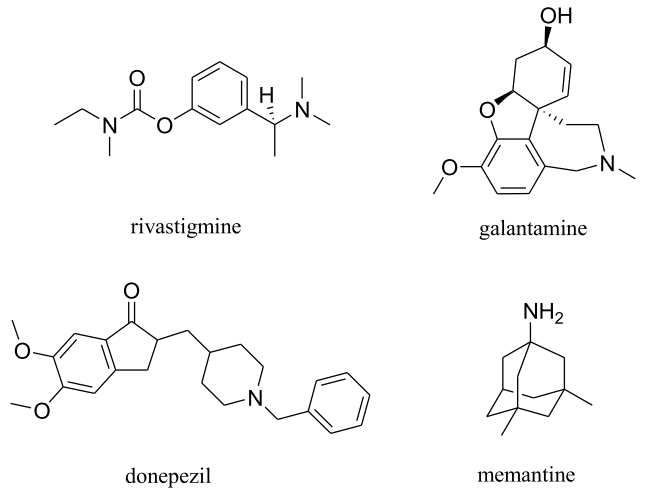

Chart 1. Currently available small molecules drugs for the treatment of AD.

modifying diseases biological drugs [7]. Their therapeutic administration was, however, reported with limitations due to the risks of serious toxic effects.

The drugs currently available for the symptomatic treatment of mild-to-moderate AD include the competitive (galantamine, donepezil) or pseudo-irreversible carbamate-based (rivastigmine) acetylcholinesterase (AChE) inhibitors (Chart 1). The impairment of cholinergic neurotransmission is a downstream process in the cognitive deficit accompanying AD, and cholinesterases inhibitors (ChEIs) have been reported to interfere with the pathogenesis and progression of AD by recovering cortical cholinergic neurotransmission and related beneficial effects on cognition [8]. Furthermore, the *N*-methyl-D-aspartate receptor (NMDAR) antagonist memantine is administered alone or in combination therapy with AChE inhibitors, since it is well known that AD patients may benefit from reduction of NMDAR and glutamate-induced Ca^{2+}-mediated excitotoxicity [9].

The aim of identifying a disease-modifying agent still represents a medical need, and trials are actually ongoing towards all the AD stages (i.e., preclinical, prodromal, and progressive), for compounds targeting Aβ- and τ-proteins, cell metabolism and bioenergetics, as well as the recovery of neurotransmission associated to cognitive decline [10,11].

The neurotransmitter ACh is mainly hydrolyzed by AChE in the synaptic cleft of the cholinergic neurons. At higher concentrations, ACh is also hydrolyzed by butyrylcholinesterase (BChE), the α-glycoprotein produced by liver and primarily distributed in plasma, but also localized in the central and peripheral nervous systems.

The exact physiological role and functions of BChE have not yet been completely understood. At present, it is known that plasma BChE is responsible for detoxification metabolism of xenobiotics [12,13], while BChE expressed and secreted in CNS glial cells and neurons likely acts as a co-regulating factor of cholinergic neurotransmission and neuroinflammation [14]. Many studies also suggested a pivotal role of BChE in onset and progression of AD [15], since the level of AChE, dominant in healthy brain, declines with disease progression, whilst a significative increase (about 30–60%) of BChE expression and activity was found in animal models and in post-mortem brain tissues analysis. Thus, a putative compensating catalytic function of BChE in the synaptic cleft is believed contributing to behavioral and cognitive dysfunction following the cholinergic deficit [16–20]. Moreover, the BChE levels resulted in high correlation with the abnormal β-amyloid (Aβ) deposition. Despite limited knowledge on mechanism linking amyloidogenesis and BChE, the selective BChE inhibitor phenethyl cymserine was reported to reduce Aβ fibrils deposition in some cerebral areas (amygdale, hippocampal structures, thalamus and basal ganglia), thus ameliorating cognitive dysfunction induced by $A\beta_{1\text{-}40}$ peptide in animal model, also affecting BChE activity in glia-mediated neuroinflammation.[21,22] Due to the enzyme distribution, the selective BChE inhibitors can represent an alternative strategy for the treatment of advanced AD, without peripheral side effects (leg cramps and gastrointestinal upset) reported for prolonged treatments with AChEIs [23,24].

AChE and BChE share about 70% of sequence homology. The active site of both enzymes is a deep and narrow gorge, and contains the high conserved catalytic triad (Ser203, His447, Glu334), the so-called oxyanion hole stabilizing the transient tetrahedral enzyme-substrate complex, and the acyl binding pocket (ABP). The choline binding pocket is buried at the bottom of the gorge, in which a residue of Trp is involved in the orientation and stabilization of choline, through cation-π interactions. Finally, the peripheral active site (PAS) is located on the rim of the active site gorge [25]. AChE and BChE mainly differ in the ABP and PAS. Two aromatic residues (Phe295 and Phe297) in the ABP of AChE are replaced by aliphatic residues (Leu286 and Val288) in ABP of BChE; six of the aromatic residues lining the AChE gorge rim and PAS are replaced by aliphatic residues in BChE, thus resulting the BChE cavity larger than AChE gorge [26–29].

Nowadays, the so-called multi-target-directed ligands (MTDL) approach is widely applied in the search for new active compounds against AD. MTDLs, which are designed by hybridization or linking design strategies, incorporate in the same molecule pharmacophore features able to simultaneously address more than one target involved in the disease onset and progression [30–33]. In MTDLs targeted to AD, the

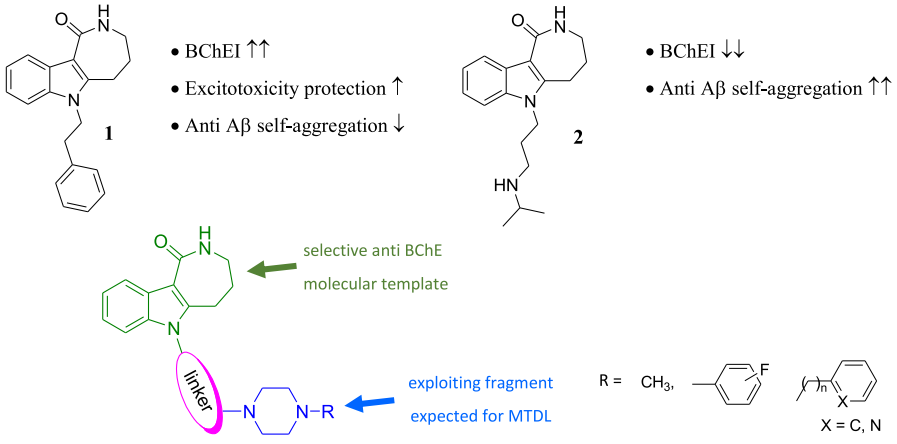

Chart 2. Design strategy for the new piperazines-containing THAI-based multitarget derivatives.

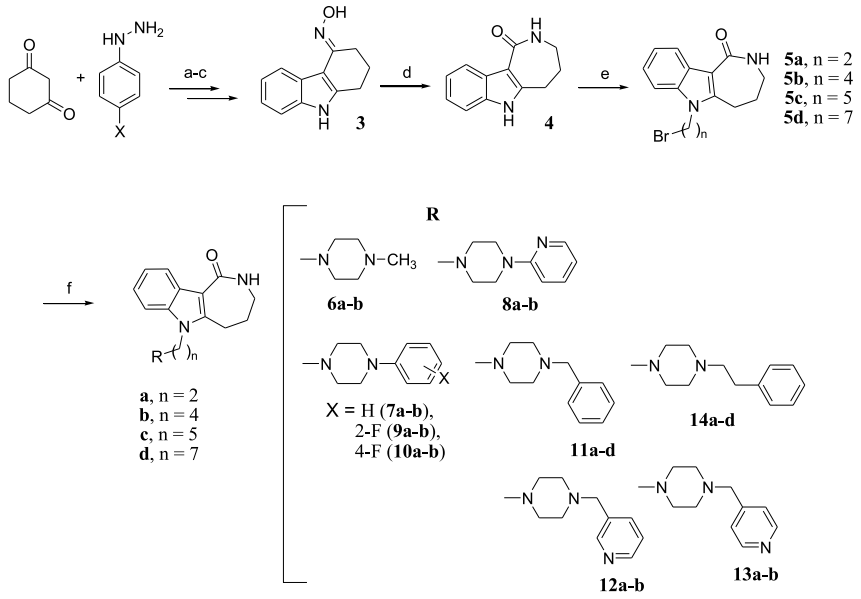

Scheme 1. a) Water, r.t., overnight, 85%; b) TFA, reflux, 24 h, 65–70%; c) $NH_2OH \times HCl$, AcONa, EtOH/H_2O 2/1 v/v, reflux, 24 h, 85–90%; d) 110 °C preheated PPA, 30 min, 70%; e) α,ω-dibromoalkane, TBAB, 25% NaOH/DCM 1/2 v/v, r.t., 48 h, 55–75%; f) piperidines/piperazines, K_2CO_3, ACN, reflux 6–10 h, 30–85%.

compounds ensure cholinesterases inhibition and additional neuroprotective activities [34].

Recently, we described 3,4,5,6-tetrahydroazepino[4,3-*b*]indol-1(2*H*)-one (THAI) as a novel scaffold of BChE inhibitors, with a promising anti-AD MTDL profile. The 6-phenylethyl THAI derivative **1** (Chart 2) proved *in vitro* a selective BChE inhibition, also endowed with additional neuroprotective activities, including protection against NMDA-induced excitotoxicity [35–38], although not so relevant as Aβ-antiaggregating agent (less than 40% at 100 μM). The replacement of the phenylethyl group by an alkylamino side chain (**2**, Chart 2) caused a sharp loss of ChEs inhibition (less than 40% of inhibition at 10 μM against both AChE and BChE) and determined a gain in the inhibition of Aβ-aggregation (50 ± 5 %, activity at 100 μM).

Piperazines are privileged fragments in medicinal chemistry, widely used as linker or interacting moiety; they are embedded as typical substructure of CNS active compounds as well as of multifunctional agents with procognitive properties [39–41]. Indeed, the bioisosteric replacement piperidine/piperazine in donepezil derivatives is effective for the development of ChEs' inhibitors; the anti Aβ-protein aggregating properties of phenyl and/or benzylpiperazines have been also described [42,43]. On the other hand, the presence of two basic nitrogen atoms in the piperazine ring improves water solubility and water/lipid partitioning properties by enhancing blood-brain barrier (BBB) crossing chances [44,45].

Herein, in the attempt to preserve BChE inhibition as well as the basic group with its physicochemical benefits, a new set of derivatives was designed by joining the THAI scaffold to different piperazine fragments through appropriate alkyl linkers (Chart 2). Therefore, we prepared a number of derivatives decorated with different 4-aryl- and 4-arylalkyl-piperazines linked an alkyl bridge anchored at to the nitrogen atom at C6 of the THAI scaffold. These new compounds were evaluated for their *in vitro* activity against cholinesterases. Molecular modelling helped to explain the molecular rationale behind the observed activity and surface plasmon resonance was employed for investigating the binding kinetics. Finally, additional cytoprotective properties against excitotoxicity and oxidative stress insults were also evaluated.

Table 1
Half maximal inhibitory concentration (IC_{50}) values (or % inhibition values at 20 μM in parenthesis)[a] of electric eel AChE and equine BChE of 3,4,5,6-tetrahydroazepino[4,3-*b*]indol-1(2*H*)-one derivatives.

Cmpd	n	IC_{50} (μM)[a]	
		AChE[b]	BChE[c]
6a	5	(20 ± 8%)	(20 ± 9%)
6b	7	15.0 ± 1.3	10.0 ± 1.1
7a	5	(31 ± 5%)	5.52 ± 1.12
7b	7	(17 ± 7%)	0.765 ± 0.050
8a	5	(13% ± 10)	0.717 ± 0.012
8b	7	9.10 ± 0.21	2.10 ± 0.11
9a	5	(35 ± 6%)	1.00 ± 0.09
9b	7	4.94 ± 1.13	0.906 ± 0.042
10a	5	(28 ± 4%)	1.78 ± 0.65
10b	7	(10 ± 5%)	10.0 ± 1.0
Tacrine[d]		0.290 ± 0.050	0.030 ± 0.005
Donepezil[d]		0.021 ± 0.009	2.30 ± 0.20

[a] Seven different concentrations of each compound were applied to determine IC_{50} values by regression of the sigmoid dose-response curves through GraphPad Prism software (release 5.01); data are mean ± SD of at least three independent measurements.
[b] Electric eel acetylcholinesterase.
[c] Horse serum butyrylcholinesterase.
[d] Tacrine and donepezil were reported as reference compounds against butyrylcholinesterase and acetylcholinesterase, respectively.

2. Results and discussion

2.1. Synthesis

THAI compounds containing piperazine moieties were synthesized as described in Scheme 1. The THAI scaffold **4** was prepared as previously reported [35–38], starting from a phenylhydrazine and 1,3-cyclohexanedione in four steps, and applying Fischer indolization and the Beckmann rearrangement of the hydroxyamino intermediate **3**. The regioselective alkylation at the indole nitrogen (N6) was achieved by stirring the suitable α,ω-di-bromo-alkanes and TBAB, as the phase transfer catalyst, in a DCM/25% aqueous NaOH biphasic mixtures, providing intermediates **5a-d**. Finally, compounds **6–14** were obtained by refluxing **5a-d** with the suitable piperazines (alkyl, aryl, benzyl, phenethyl) and potassium carbonate in acetonitrile. Where not

Table 2
Half maximal inhibitory concentration (IC_{50}) values (or % inhibition values at 20 μM in parenthesis)[a] of electric eel AChE and equine BChE of 3,4,5,6-tetrahydroazepino[4,3-*b*]indol-1(2*H*)-one derivatives.

Cmpd	n	IC_{50} (μM)[a]		Aβ aggregation % inhibition[f]
		AChE[b]	BChE[c]	
11a	2	6.57 ± 0.65	6.59 ± 0.71	13 ± 4%
11b	4	1.48 ± 0.35	2.64 ± 0.27	
11c	5	1.83 ± 0.26	0.430 ± 0.011	28 ± 6%
11d	7	0.402 ± 0.015	0.396 ± 0.022	
12a	5	(37 ± 1%)	4.92 ± 0.44	
12b	7	(40 ± 2%)	0.466 ± 0.021	
13a	5	(2 ± 2%)	1.92 ± 0.19	
13b	7	7.06 ± 0.19	1.86 ± 0.35	
14a	2	(8 ± 3%)	5.79 ± 0.13	55 ± 7%
14b	4	(36 ± 4%)	0.528 ± 0.032	21 ± 5%
14c	5	(39 ± 5%) [20 ± 3%][e]	0.163 ± 0.023 [0.190 ± 0.011][e]	14 ± 5%
14d	7	5.90 ± 0.22 [39 ± 7%][e]	0.065 ± 0.009 [0.072 ± 0.011][e]	62 ± 5%
Tacrine[d]		0.290 ± 0.050 [0.090 ± 0.009][e]	0.030 ± 0.005 [0.025 ± 0.003][e]	
Donepezil[d]		0.021 ± 0.009 [0.018 ± 0.002][e]	2.30 ± 0.20 [5.10 ± 0.50][e]	
Quercetin[f]				82 ± 7%

[a-d] See footnotes in Table 1.
[e] Human enzymes isoforms.
[f] Inhibition of self-induced Aβ aggregation, at the final concentration of 100 μM. Quercetin was tested as reference compound.

commercially available, piperazines were synthesized by applying synthesis described elsewhere.

2.2. Cholinesterases inhibition assays

The *in vitro* activity of the new compounds was measured toward horse serum (*hs*) BChE and electric eel (*ee*) AChE, by applying the Ellman colorimetric assay, with slight modifications [46]. All derivatives were first tested at a single point 2×10^{-5} M concentration, and those showing, at least, 60% inhibition were further tested to determine their half-maximal inhibitory concentrations (IC_{50} values). Tacrine and donepezil were tested as positive controls against BChE and AChE, respectively.

Table 3
Squared correlation matrix of the coefficient of determination (R^2) of the *eq* BChE's inhibition data (pIC_{50}) and physicochemical descriptors.

	eq BChE	ClogP	$LogP_{acd}$	Log D	MR	MV
***eq* BChE**	1					
ClogP	0.431	1				
$LogP_{acd}$	0.343	0.641	1			
Lod D	0.341	0.680	0.992	1		
MR	0.706	0.690	0.430	0.453	1	
MV	0.709	0.737	0.528	0.549	0.975	1

According to previously reported results [35–38], the THAI moiety emerged as the molecular determinant for a selective inhibition of BChE with only few exceptions.

Compounds bearing the *N*-methylpiperazine (**6a**) fragment, linked to the THAI scaffold by a *n*-pentyl spacer, resulted less active than the higher *n*-heptyl homologue against both ChEs (Table 1). A shorter linker from 2 to 4 methylene groups also led to inactive derivatives (data not shown). By maintaining the *n*-pentyl chain, an increased activity against BChE was achieved by introducing the unsubstituted *N*-phenylpiperazine fragment, which returned compound **7a** as a moderate BChE inhibitor. The 2-pyridylpiperazine congener (**8a**) was 2-3-fold more active than **7a**, suggesting a positive contribution of electron withdrawing substituents. This was confirmed by introducing a fluorine substituent on the *ortho* position (**9a**). In contrast, only a slight increased activity was observed in the corresponding *para* substituted fluorine congener (**10a**).

The elongation of the spacer to *n*-heptyl chain enhanced cholinesterases inhibition in both *N*-methyl (**6b**) and *N*-phenyl piperazine (**7b**) derivatives, mostly towards BChE. However, with only the exception of the *ortho*-F-substituted derivative **9b**, which retained anti BChE activity of its C5 congener (**9a**), the 2-pyridyl derivative (**8b**) showed a reduced efficacy as well as the *para*-F-phenyl analogue (**10b**). Noteworthy, a moderate AChE inhibition was achieved only by combining a *n*-heptyl spacer along with *ortho*-substituted phenylpiperazines containing electron withdrawing groups.

Further modifications were explored by introducing benzyl or phenethyl substituents on piperazine ring, as reported in Table 2.

Derivatives **11a-d** exhibited a moderate inhibition of both BChE and AChE, with IC_{50} values in the low micromolar range. The elongation of the alkyl spacer from 2 to 5 methylene units did increase BChE inhibition. However, a longer alkyl chain did not provide any further improvement, thus showing compounds **11c** (n = 5) and **11d** (n = 7) a comparable activity. Compound **11a** (n = 2), and **11b** (n = 4) were, respectively, from 1.5 to 1 order of magnitude less active than **11c** and **11d**. Inhibition of AChE remained unvaried when *n*-butyl (**11b**) and *n*-pentyl (**11c**) spacers were explored but was enhanced by increasing the alkyl chain length till seven methylene units. Compound **11d** was identified as a dual cholinesterases inhibitor, thus proving inhibition of both AChE and BChE in the same range of concentrations.

Substituting the benzylpiperazine by a pyridinylmethyl piperazine, a significant BChE inhibition was achieved only in 3-pyridinylmethyl derivative **12b** (IC_{50} = 0.466 μM), bearing a *n*-heptyl spacer. A shorter linker or a 4-pyridinyl group were unfavorable. Moreover, the

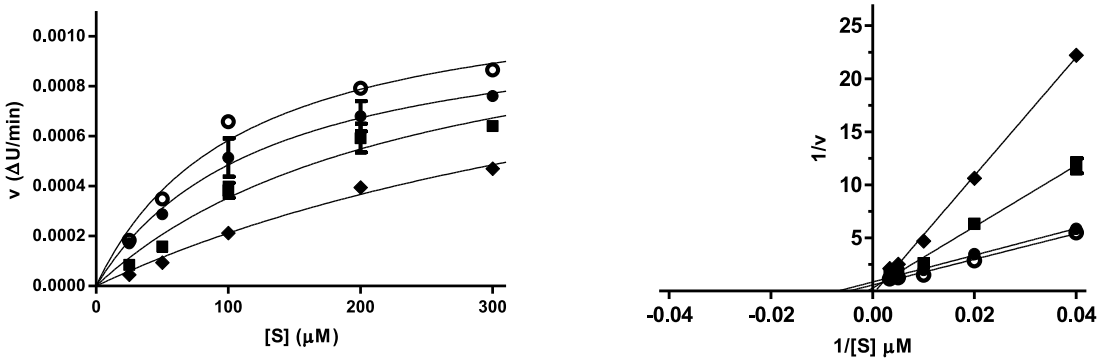

Fig. 1. Inhibition kinetics (letf) and Lineweaver–Burk plot (right), R^2 = 0.978–0.998 for *eq*BChE (0.18 U/mL) and **14d** (0–200 nM) by using different substrate (butyrylthiocholine iodide) concentrations (50–300 μM). (◯) no inhibitor, (●) 50 nM, (■) 100 nM, (◆) 200 nM.

Table 4
Affinity and kinetic data from SPR for the binding of selected compound to *eq*BChE.

Cmpd	K_D (nM)[a]	k_{on} ($M^{-1}s^{-1}$)[b]	k_{off} (s^{-1})[c]	τ (s)[d]
7b	759 ± 15	4.49 (±0.80) × 10^4	0.0341 ± 0.0005	30
14c	148 ± 6	8.21 (±0.80) × 10^5	0.1229 ± 0.0010	8
14d	62 ± 2	3.43 (±0.05) × 10^5	0.02142 ± 0.0055	47
Tacrine	49 ± 2	4.92 (±0.10) × 10^5	0.02705 ± 0.0011	37
Donepezil	7200 ± 235	1.24 (±0.20) × 10^4	0.1376 ± 0.0022	7

[a] Equilibrium dissociation constants (K_D). Data represent mean ± SD values of at least three different experiments.
[b] Kinetic association rate constant (k_{on}).
[c] Kinetic dissociation rate constants (k_{off}).
[d] Residence time ($\tau = 1/k_{off}$).

replacement of benzyl by a phenethyl group improved BChE inhibition. Except for **14d**, which achieved IC_{50} of 5.90 μM, the *N*-phenylethyl congeners showed less than 50% AChE inhibition at 20 μM. Again, BChE inhibition increased by increasing the alkyl linker length: ethyl (**14a**) < *n*-butyl (**14b**) < *n*-pentyl (**14c**) < *n*-heptyl (**14d**). Compounds **14c** (IC_{50} = 163 nM) and **14d** (IC_{50} = 65 nM) turned out as the most potent BChE inhibitors in the series. Overall, due to the larger volume of BChE gorge containing the active site, we can deduce that bulkiness properties mainly affected enzyme inhibition. As shown in Table 3, a satisfactory correlation was observed between BChE inhibition data (n = 22 compounds) and only in the case of molar volume (Supp. Info. Fig. S1, R^2 = 0.709) and molar refractivity (R^2 = 0.706), i.e., two parameters describing bulkiness/polarizability of the organic molecules.

The mechanism of the BChE inhibition of the most potent BChE inhibitor **14d** was studied. The Lineweaver-Burk curves were derived by using a fixed amount of BChE (0.18 U/ml) and varying concentrations of the substrates between 25 and 300 μM, in the absence or presence of inhibitor at different concentrations (0.05–0.5 μM). Binding of **14d** to BChE changed both V_{max} and K_m values, a trend that is generally ascribed to mixed-type inhibition (Fig. 1). A replot of the slopes versus the corresponding inhibitor concentrations (Supp. Info. Fig. S2) provided a K_i value of 27 nM.

The inhibitory activity of **14c-d** was further evaluated against human isoforms of AChE and BChE (Table 2), but not any significant species-dependent difference was observed in the inhibition activity.

2.3. BChE binding kinetics through surface plasmon resonance

Drug effectiveness is determined by combination of mechanism of action, affinity, and binding kinetics defined by association (k_{on}) and dissociation (k_{off}) rate constants, which define the time course of target occupancy and residence time (τ). A faster association rate speeds up the onset of action, while a slower dissociation prolongs it. Moreover, the side effects could arise from a prolonged target blocking or off-target interactions, often enhanced by magnitude and frequency of dosing [47]. Thus, optimizing both affinity and kinetic profile in early stages of drugs design and development is advantageous in balancing efficacy and safety [48].

By applying surface plasmon resonance (SPR) technology, we compared binding kinetics of compounds **14c** and **14d** to immobilized equine BChE. Lacking detailed protocols, describing the SPR immobilization of BChE, and inspired by SPR analysis of AChE inhibitors,[49,50] we investigated different experimental conditions to generate a stable and high-density biosensor by amine coupling. Taking into account the BChE isoelectric point (pI = 6.5), as well as covalent coupling requires

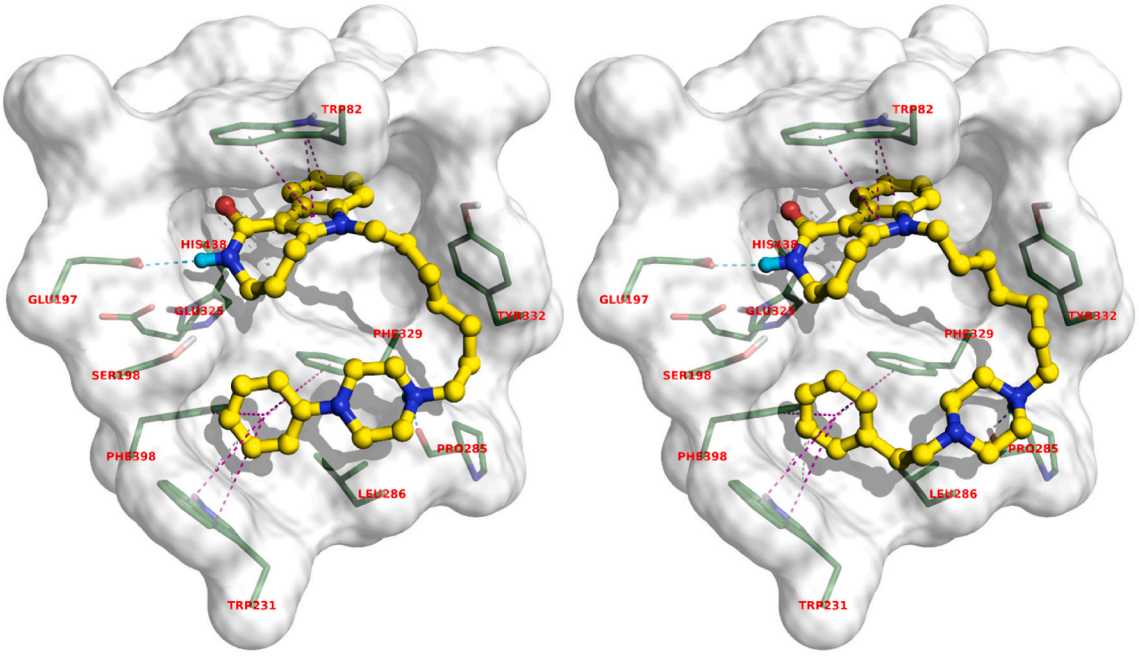

	FEB[(a)]	ΔE[(b)]	EFF[(c)]	TAN[(d)]	POP[(e)]
7b	–8.17	0.34	–0.240	0.703	20/100
14d	–9.62	0.07	–0.267	0.713	31/100

Fig. 2. Binding mode and docking scores for **7b** (left) and **14d** (right) into the BChE active site. H-bonds and π-π stackings are depicted in cyan and magenta dashed lines, respectively. [(a)]FEB Free Energy of Binding. [(b)]ΔE Energy difference between the selected pose and the relative global minimum. [(c)]EFF Ligand efficacy. [(d)]TAN Tanimoto_Combo similarity coefficient with TKN X-ray pose. [(e)]POP Cluster members population.

acid (pH ≈ 5) and low ionic-strength conditions to achieve efficient protein electrostatic pre-concentration on sensor surface, we first investigated BChE activity after a pre-incubation in pH 4.5 buffered solution (pH ≤ pI - 1.5 units), in order to ascertain the applied experimental conditions did not negatively affect both enzyme activity and stability. After 30 min incubation (protein concentration 50 U/mL) under two different pH 4.5 buffered conditions (10 mM sodium acetate and 10 mM sodium dihydrogen phosphate, respectively), changes in enzyme activity and substrate affinity were not observed (Supp. Info. Table S3). On this basis, a 10 mM sodium acetate solution (pH = 4.5) was accepted for protein activation. According to optimal working pH of BChE (pH = 7.5–8), a 10 mM phosphate pH = 8 buffered solution was selected as run buffer, and the effect of surfactant addition was evaluated (Table S4). Although BChE has been reported as a not surfactant dependent enzyme [51], we verified that supplementation with 0.05% of Triton X-100 reduces both substrate affinity (one magnitude order) and rate constant (five times); only a slight increase of BTC affinity, without effects of enzyme reaction rate, were observed by supplementation with 0.05% of polysorbate P20. Based on these results, we decided to avoid surfactants addition in run buffer solution. BChE immobilization was carried out on a COOH-V sensor chip surface, preactivated by injecting 200 μL of a 1/1 v/v mixture of NHS (0.1 M) and EDC (0.4 M) at 25 μL/min flow rate, followed by injecting 250 μL of three different solutions containing equine BChE (50 U/mL in 10 mM acetate pH = 4.5 buffered solution) at 25 μL/min flow rate. The capping of activated but unreacted carboxyl sites was obtained by flowing overnight a 50 mM TRIS (pH = 8) buffered solution, as a milder quenching procedure rather than 1 M ethanolamine solution, that in the first attempt largely removed protein from the sensor surface. The efficacy of immobilization was proved by 10 repeated injections of 3 M NaCl as regenerating solution, without a significant loss of protein. The reference channel on the sensor was prepared by applying the same protocol apart from enzyme injection. After immobilization process, a 6500 RU apparent enzyme immobilization grade was estimated, employing tacrine, and donepezil as test compounds. Binding studies were carried out at 25 μL/min as flow rate, whilst injections of running buffer solution (10 mM PB, pH = 8) was used as 'blank' for the so-called double-referencing. Each interaction was analyzed at least in triplicate, thus showing high data reproduction (Table 4).

All the K_D values were found according to their BChE inhibition potencies (IC_{50} values). By applying the global fitting equation, the association (k_{on}) and dissociation (k_{off}) rate constants were obtained with good approximation, and the residence times (τ) calculated from k_{off} values (Supp. Info. Fig. S5).

Compound **14d** exhibited a kinetic binding profile comparable to that of tacrine, by showing a quite similar association rate k_{on}, and only slightly different dissociation rate k_{off}, which resulted in a residence times τ = 47 s for **14d**, and τ = 37 s for tacrine, respectively. Results seem to suggest a potential for efficacy and duration of action for **14d**, which achieved a good target occupancy, a relatively fast association rate and slow dissociation ones.[52,53] The most lipophilic derivative **7d**, yet bearing the *n*-heptyl chain linker and the *N*-phenylpiperazine fragment, though k_{on} and k_{off} values slight similar to that of **14d** and tacrine, resulted in a dramatic loss in affinity. Compound **14c**, bearing the *n*-pentyl spacer, was confirmed two-fold less active than **14d**; from a kinetic point of view, it exhibited a two times faster equilibration with the target, followed by a five times most rapid dissociation (**14c**, τ = 8 s).

2.4. Molecular modelling

To provide a critical evaluation of the observed differences in the BChE inhibition potency, the binding mode of compounds **7b** and **14d** to BChE was investigated by molecular docking simulations (Fig. 2). To this end, we started for more than one evidence reporting highly puckered conformations in ligands binding to the BChE active site reported in several X-ray complexes, including the data referring to a potent tacrine-methyl-anacardate hybrid ligand **TKN** [54], taken hence as a template for the assessment of docking results. In comparing dockings of **7b** and **14d**, we mainly focused on the correspondence of the binding interaction patterns of the two compounds and **TKN**, especially with respect to the critical hotspots (CAS, PAS and ABP), as well as on the increase in ligand affinity caused by the elongation of the alkyl linker joining the THAI scaffold to the decorated piperazine fragment.

Compounds **7b** and **14d** both complete the inner part of the enzyme binding site, with the THAI scaffold being able to recruit a hydrogen bond involving the Glu197 near the catalytic triad and to make face-to-face π−π stacking with the indole part of CAS Trp82, as is the case for the tacrine ring in the X-ray complex [54].

	FEB[a]	ΔE[b]	EFF[c]	TAN[d]	POP[e]
7b	−8.17	0.34	−0.240	0.703	20/100
14d	−9.62	0.07	−0.267	0.713	31/100

It appeared that in both poses the water molecules do not contribute to the stabilization of the enzyme-ligand complex. The flexibility of *n*-

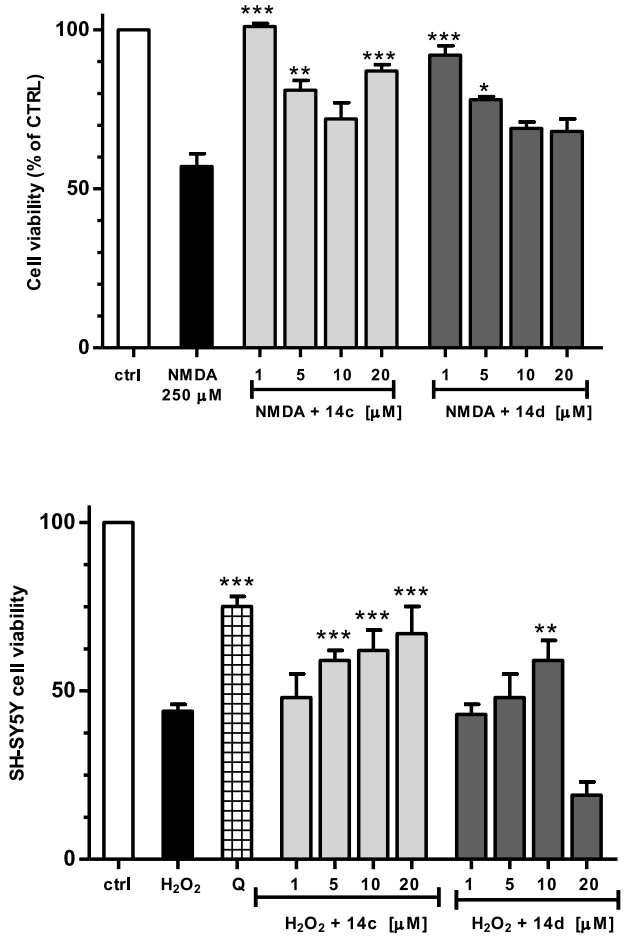

Fig. 3. The cytoprotective effect of compounds **14c** and **14d** against NMDA toxic applied insult (top panel), or H_2O_2-induced oxidative insult (bottom panel) on neuroblastoma cell line SH-SY5Y. The test compounds, at dose ranking from 1 to 20 μM, were co-incubated 24 h with 250 μM NMDA or 80 μM H_2O_2. respectively, and cell viability was assessed by MTT test and referred to control cells. Quercetin (Q) at 100 μM was used as antioxidant standard control. Each bars represent mean ± SD of at least three independent experiments. Statistical analysis was done by applying one-way ANOVA followed by multiple comparison tests (Dunnett's test). Levels of significance: ***$p < 0.001$, **$p < 0.01$, *$p < 0.05$ vs NMDA or H_2O_2 alone.

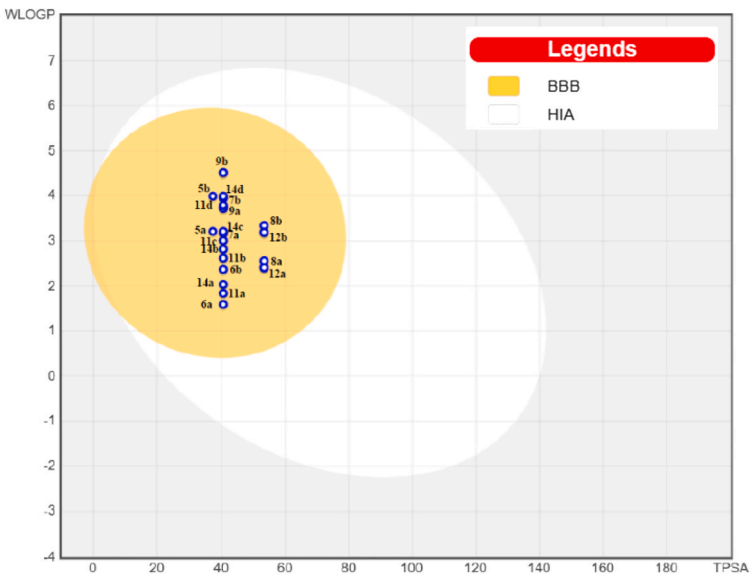

	14c	14d
BBB penetration[a]	+	+
HIA[b]	+	+
HT[c]	-	-

Fig. 4. Predicted pharmacokinetic properties of newly synthesized piperazine-containing THAI derivatives, according to BoiledEgg model. [a]BBB = blood–brain barrier permeation; [b]HIA = human intestinal absorption. [c]Hepatotoxicity (AdmetSAR). Detailed data for **14c**, and **14d** are reported in the table.

heptyl linker allows the right bending to complement the shape of the edge entrance of the active site bounded by Tyr332. The terminal aryl-piperazine moieties attain additional interactions, in particular the hedge-like π–π stacking with residues Trp231, Phe239 and Phe398 of the PAS, as well as less extended hydrophobic contacts with the Val286 residue of the ABP. Moreover, the charged nitrogen atom of the piperazine ring enhances the stabilization of the enzyme-inhibitor complex by a reinforced H-bond with the backbone of Pro285, an interaction which freezes the folding of the entire scaffolds in a highly curved arrangement, which can then almost completely fill the gorge of the BChE active site. As far as the most active compounds **14d** is concerned, it might be argued that the piperazine fragment bearing the longer phenethyl group could generate a more thermodynamically efficient folding keeping longer the ligand buried into the active site gorge. Indeed, better docking scores were gained for this ligand with respect to **7b** once the ESP selection rule is applied to filter out docking poses (see Methods). The applied ranking metrics, especially with FEB and EFF, might help at least in part in a plausible interpretation of the observed IC_{50} data differences. In addition, the reliability of THAI docking poses is also proved by the overlap with available X-ray (Supp. Info. Fig. S6) binding modes.

2.5. Additional neuroprotectant effects

2.5.1. $A\beta_{1\text{-}40}$ aggregation assay

Small molecules able to induce inhibition of Aβ aggregation/neurotoxicity and ChEs simultaneously may a have therapeutic potential as anti-AD agents. BChE inhibitors **11a-d** and **14a-d** were assayed for their properties to affect and inhibit the $A\beta_{1\text{-}40}$ self-induced aggregation, through a test measuring thioflavin T (ThT) fluorescence [53]. Quercetin, as a strong *in vitro* inhibitor of Aβ aggregation, was tested as positive control. All the tested compounds were less active than quercetin, showing % inhibition at 100 μM concentration ranging between 15% and 62%, without any apparent dependence upon the structure properties. Compound **14d** showed the highest activity (62% of inhibition). The anti-Aβ pharmacophore has been established by a planar heterocyclic scaffold, as an intercalating moiety for disruption of β-sheet secondary structure, decorated with suitably small polar and H-bonding groups. Likely, the lower activity of tested compounds may be mainly determined by the lack of these groups in suitable positions [37].

2.5.2. Cell viability in neuronal cells

The most interesting derivatives **14c** and **14d** were tested for their intrinsic cytotoxic effects, by exposing human neuroblastoma cell line (SH-SY5Y) at increasing concentrations (from 1 to 100 μM) of the test compounds. The cell viability was assessed by applying the (3,4,5-dimethylthiazol-2-yl)-2,5-diphenyltetrazolium bromide (MTT) assay, after 24 h of co-incubation. Both derivatives showed a dose-dependent effect, causing cytotoxicity only at a dose higher than 50 μM (**14c** $IC_{50} = 88 \pm 4$ μM; **14d** $IC_{50} = 60 \pm 5$ μM, respectively), thus two orders of magnitude higher than that causing *in vitro* inhibition of BChE (Supp. Info. Fig. S7). Compounds **14c**, and **14d** were further studied for their *in vitro* efficacy to counteract the NMDA-induced toxicity and H_2O_2-induced oxidative insult in SH-SY5Y cells line (MTT assay, Fig. 3). The neuronal cells were exposed to the insults and to the co-treated cells with increasing concentrations (from 1 to 20 μM) of the tested compounds.

NMDA decreased viability of the cells by about 40% at the final concentration of 250 μM. After co-incubation with **14c** and **14d**, cell viability was significantly recovered ($P < 0.001$) at the lowest concentration tested (1 μM). A loss of protective effect against NMDA-induced cytotoxicity between 20 and 30% was observed at concentrations equal to or greater than 5 μM for both **14c** and **14d** (Fig. 3, top panel), which showed statistically significant effects at 5 μM (and **14d** at 20 μM). The lack of a clear dose-response relationship is not unexpected when determining protective effects from toxic insults. The trend observed in the top panel of Fig. 3 may suggest the impact of their own cytotoxicities at concentrations higher than 5 μM and/or a lower specificity of the cell response (i.e., activation of protective mechanisms other than the NMDA antagonism) at the highest concentration of 20 μM as in the case of **14c**. While the assessment of the modulatory effects on the NMDA receptor needs more specific and in-depth investigation, here we can highlight that compounds **14c** and **14d** show their own toxicity towards neuronal cells at concentrations several hundred times (i.e. 500 and 800 times, respectively) higher than their IC_{50}s towards BChE, whereas protect the neuronal cells from the 250 μM NMDA cytotoxic insult at 1 μM, that is at least sixtyfold lower concentrations than their cytotoxic IC_{50}s.

The cytoprotective effect on SH-SY5Y cell line against H_2O_2-induced oxidative insult (Fig. 3, bottom panel), was further investigated, using the natural antioxidant quercetin as positive control. Compound **14c** exhibited a statistically significant dose-dependent effectiveness at concentrations higher than 5 μM, reaching at 20 μM a protection comparable to that of quercetin at 100 μM concentration. The calculated

Table 5
THAI derivatives water solubility and binding to HSA.

Cmpd	HSA binding[a]		
	K_D (μM)	k_{off} (sec^{-1})	τ (sec)
1	0.85 ± 0.10	0.0166	60
7b	1.64 ± 0.40	0.06865	15
14c	6.70 ± 0.21	0.0920	11
14d	3.53 ± 0.42	0.1510	6
warf[b]	5.50 ± 0.33		

[a] Binding to immobilized human serum albumin (HSA). Reported values: equilibrium dissociation constants (K_D), dissociation rate constants (k_{off}), residence time (τ).

[b] Experimental K_D for the reference drug warfarin (warf); value according to that previously reported [38].

EC_{50} was approximatively equal to 1.5 μM. Compound **14d** reversed its cytoprotective effect at the highest concentration (20 μM), most likely due to its own impact on cell viability at higher doses.

As a matter of fact, **14c** and **14d** were not effective when tested by *in vitro* evaluation of chemical quenching of the ROS production (efficacy <10%), suggesting lack of scavenging activity (data not shown). The protection showed in cell assays seems to suggest that the cytoprotective effect against H_2O_2-induced insults could not exclude activation of cellular mechanisms interfering with pathways of cell death machinery activated by ROS insult (NF-κB, MAPK, DNA damage, lipid peroxidation, mitochondrial membrane dysfunction, autophagy, calcium homeostasis destruction, caspase cascade activation) [55].

2.6. ADME-related physicochemical properties

The experimental water solubility of compound **14c** and **14d** was measured by applying the previously described method [56]. Each compound was incubated at pH 7.4 and 25 °C, at a saturating concentration, in 0.1 M phosphate buffered solution (PB) also containing 0.15 M of KCl. All derivatives exhibited a water solubility higher than predicted by SwissADME and ACDLabs suite software in the same pH buffered solutions (Supp. Info. Table S8).

Compound **14c** (s = 169 ± 1 μg mL^{-1}) was found significantly more soluble than **14d** (s = 6.1 ± 0.1 μg mL^{-1}) under the same experimental conditions, and about one order of magnitude higher than predicted. By following the solubility ranking commonly reported, compound **14c** resulted as a soluble compound, whereas **14d** was ranked as moderately/poor soluble [57].

A preliminary in silico prediction of the oral bioavailability and BBB crossing, relevant for the likelihood that CNS directed compounds could be effective, was made. Compounds **14c** and **14d** did not show violation of the Lipinski's rule, even applying more strict filter criteria for CNS drug candidates (MW < 450, clog P < 5, number of hydrogen bond donors HBD <3, number of hydrogen bond acceptors HBA <7, and polar surface area PSA <60–70). The BOILED-Egg plot [58] predicted all the newly synthesized compounds as well absorbed and distributed across BBB, as depicted in the yellow ellipse of Fig. 4. The same results were also predicted by applying AdmetSAR software [59], which also returned the compounds as not hepatotoxic.

Finally, the interaction with HSA was estimated by surface plasmon resonance (SPR) using the well-known HSA strong binder warfarin as standard references. [38].

HSA represents the most abundant protein in plasma and plays a relevant role in affecting the ADME profiles of xenobiotics. The binding curves showed the responses at equilibrium were quite rapidly reached for each of tested compounds. By applying the global fitting refinement, the kinetic dissociation rate constants from HSA were obtained with good approximation, and the residence times calculated. By considering the physiological HSA concentration in plasma (680 μM), at 10 μM concentration all compounds were predicted highly bound to albumin [38]. Lipophilicity mainly affected the affinity profile, and piperazine derivatives exhibited a 2–8 fold lower HSA binding than compound **1**, thus suggesting an enhanced free bioactive fraction in plasma (Table 5). Compound **14c** (K_D = 6.70 μM) showed a weaker affinity than the two analogues **7b** and **14d**. The most lipophilic derivatives **7b** (K_D = 1.64 μM) and **14d** (K_D = 3.53 μM) exhibited a quite similar affinity than warfarin, taken as a reference compound. From a kinetic point of view, compound **14d** proved k_{off} dissociation rate constants two times faster than analogues **7b** and **14c**, which resulted in a very shorter residence time (τ = 6.5 s), thus characterizing the behavior of **14d** as a fast reversible binder, which can positively affect the distribution/activity profile.

3. Conclusions

Following our previous studies, twenty-two new THAI derivatives were designed and prepared by introducing alkyl chain bearing differently decorated piperazine fragments. Evaluated *in vitro* as inhibitors of ChEs, the newly synthesized compounds showed selective inhibition of BChE, with the only exception of compound **11d**, which appeared as dual AChE/BChE inhibitor. Molar volume and molar refractivity were the physicochemical parameters mainly associated to the variation of the inhibition potency. The most potent derivatives **14c** (*eq*BChE IC_{50} = 163 nM) and **14d** (*eq*BChE IC_{50} = 65 nM) exhibited BChE-selective inhibition in the nanomolar range of concentrations, also achieving similar IC_{50}s towards the human ChEs isoforms. Compound **14d** behaved as a mixed-type inhibitor.

In depth investigation of kinetics of binding with BChE and residence time proved that the design strategy achieved a promising potency, as well as a long residence time for drug-target complex, thus suggesting an increased duration of efficacy, and a reduction in potential off-target side effects, which often limits the prolonged therapeutic administration of ChEs inhibitors.

Molecular docking calculation suggested that the flexible *n*-heptyl linker could promote the occurrence of a bent pose filling the throat of the BChE active site and, more importantly, even more tightly fitting the binding site of BChE.

Compounds **14c**, and **14d** did not exhibit cytotoxicity at doses allowing enzyme inhibition, also showing at 1 μM concentration a significant ($P < 0.001$) protection of neuroblastoma SH-SY5Y cell line against insults induced by NMDA or oxidative stress (hydrogen peroxide). Finally, compound **14d** achieved additional inhibition of *in vitro* self-assembling Aβ protein. Taking these properties into account, the presented compounds can be considered valuable hits for developing new BChE inhibitors endowed of potential as MTDL in the management of multifactorial AD-related neurodegeneration. Among them, **14d** represents a new promising candidate for further *in vivo* pharmacological studies and molecular optimization to ameliorate activity and druggability.

4. Materials and methods

Starting materials and all chemicals and solvents were purchased from Sigma-Aldrich and Alfa Aesar. Melting points were determined by using the capillary method on a Stuart Scientific SMP3 electrothermal apparatus and are uncorrected. Final compound purities were assessed by elemental analyses (C, H, N), performed on Euro EA3000 analyzer (Eurovector, Milan, Italy) by the Analytical Laboratory Service of the Department of Pharmacy-Drug Sciences of the University of Bari (Italy), and the results agreed to within:0.4% of theoretical values. All the tested compounds showed a higher than 95% purity. Mass spectra were obtained by Agilent 1100 Series LC–MSD Trap System VL, equipped with ESI (electrospray ionization) source. The high-resolution molecular masses of test compounds were assessed by Agilent 6530 Accurate Mass Q-TOF spectrometer (Agilent Technologies). IR spectra (KBr disks) were recorded on a Spectrum One FT infrared spectrophotometer

(PerkinElmer), and the most significant absorption bands are listed. 1H NMR spectra were recorded at 300 MHz on a Varian Mercury 300 instrument. Chemical shifts data are expressed in δ and the coupling constants J are in hertz (Hz); the following abbreviations are used for multiplicity: s, singlet; d, doublet; dd, doublet-doublet; td, triplet of doublets; t, triplet; q, quartet; m, multiplet. Signals due to NH and OH protons were located by deuterium exchange with D_2O. Chromatographic separations were performed on silica gel 60 for column chromatography (Merck 70–230 mesh).

Dulbecco's modified Eagle's medium high glucose (DMEM), fetal bovine serum (FBS), penicillin, L-glutamine, streptomycin and trypsin were purchased by Euroclone (Italy); 3-(4,5-dimethylthiazol-2-yl)-2,5-diphenyltetrazolium bromide (MTT) was provided from Invitrogen (Thermo Fisher Scientific, USA).

4.1. Synthesis

4.1.1. General procedure A: preparation of 6-ω-bromoalkyl-2,3,4,5-tetrahydroazepino [4,3-b]indol-1(6H)-one derivatives (5a-d)

The preparation of 6-(4-bromobutyl)-2,3,4,5-tetrahydroazepino[4,3-*b*]indol-1(6*H*)-one (**5b**) has been reported as a representative example.

To a solution containing 200 mg (1 mmol) of 2,3,4,5-tetrahydroazepino[4,3-*b*]indol-1(6*H*)-one **3**, prepared as previously reported [35], in 20 mL of methylene chloride (DCM) were added 0.84 mL (7 mmol) of 1,4-dibromo-butane, 322 mg (1 mmol) of tetrabutyl ammonium bromide (TBAB), and 10 mL of 25% w/v aqueous NaOH. After the mixture was stirred overnight at room temperature, were added 20 mL of fresh methylene chloride and 20 mL of water, and the mixture was shook in a separatory funnel. The organic phase was collected, washed five times with 20 mL of water, dried over anhydrous Na_2SO_4, and concentrated under reduced pressure. The obtained oil was washed by treating it 5 times with 10 mL of *n*-hexane. The final residue was purified by chromatography on silica gel, by eluting with a *n*-hexane/ethyl acetate (7/3, v/v) mixture as a mobile phase. The intermediate compound **5b** was obtained as a brow oil, which was used without further purification. Yield: 62% (220 mg). IR (KBr) ν: 3265, 3188, 3038, 2937, 1627 cm^{-1}. ^1H NMR (300 MHz, $CDCl_3$) δ: 8.27 (d, $J = 8.0$ Hz, 1H), 7.45 (t, $J = 7.0$ Hz, 1H), 7.30 (d, $J = 8.0$ Hz, 1H), 7.11 (t, $J = 8.0$ Hz, 1H), 6.89 (t, $J = 5.0$ Hz, 1H), 4.12 (t, $J = 6.0$ Hz, 2H), 3.20–3.16 (m, 4H), 3.18 (t, $J = 7.0$ Hz, 2H), 2.10–2.00 (m, 2H), 1.80–1.65 (m, 4H).

4.1.2. General procedure B: preparation of 6-(piperazin-1-yl)alkyl)-2,3,4,5-tetrahydroazepino [4,3-b]indol-1(6H)-one derivatives (5–14)

The preparation of *2,3,4,5-tetrahydro-6-[7-(4-phenylpiperazin*-1-yl*) heptyl]azepino* [*4,3-b*]*indol-1(6H)-one* (***7b***) has been reported as a representative example.

To a suspension of compound **4d** (378 mg, 1 mmol) in 10 mL of dry acetonitrile (ACN) were added anhydrous K_2CO_3 (415 mg, 3 mmol), and 1-phenylpiperazine (0.23 mL, 1.5 mmol). The mixture was refluxed 6 h, until the disappearance of **4d**. After cooling, the solvent was removed under reduce pressure and the obtained oil was suspended in 25 mL of water and extracted twice with 20 mL of methylene chloride. The collected organic phases were dried over anhydrous Na_2SO_4, and concentrated under reduced pressure. The obtained residue was purified by chromatography on silica gel, by eluting with a methylene chloride/methanol (95/5, v/v) mixture as a mobile phase. Compound **7b** was obtained as a pale brown solid. Yield: 55% (252 mg). M.p. 146–148 °C. IR (KBr) ν: 3417, 3263, 3177, 3037, 2927, 1626, 1599, 1464, 1440, 1233, 757, 731, 668 cm^{-1}. ^1H NMR (300 MHz, CDCl3) δ: 8.45–8.39 (m, 1H), 7.33–7.18 (m, 6H), 6.92 (dd, $J1 = 7.9$ Hz, $J2 = 2.2$ Hz, 2H) 5.98 (t, $J = 5.5$ Hz, 1H), 4.08 (t, $J = 7.5$ Hz, 2H), 3.46–3.28 (m, 6H), 3.09 (t, $J = 6.5$ Hz, 2H), 2.94–2.79 (m, 2H), 2.65–2.55 (m, 2H), 2.27–2.15 (m, 2H), 1.83–1.62 (m, 2H), 1.43–1.26 (m, 6H). ^{13}C NMR (101 MHz, $CDCl_3$) δ 169.0, 151.3, 141.3, 136.2, 129.1, 128.2, 122.6, 122.4, 121.4, 119.7, 116.0, 108.8, 107.0, 58.7, 53.3, 49.1, 43.4, 41.5, 29.7, 29.3, 27.4, 27.3, 27.0, 26.9, 26.8. HRMS (ESI-MS) *m/z*: $[M+H]^+$ calcd for $C_{29}H_{39}N_4O$: 459.3118, found: 459.3121. Anal $C_{29}H_{38}N_4O$ (C, H, N).

4.1.3. 2,3,4,5-Tetrahydro-6-(5-(4-methylpiperazin-1-yl)pentyl)azepino [4,3-b]indol-1(6H)-one (6a)

Compound **6a** was obtained as a brown oil, by starting from **4c** (380 mg, 1 mmol), anhydrous K_2CO_3 (415 mg, 3 mmol), and 1-methyl-piperazine (0.2 mL, 1.5 mmol). Yield: 61% (224 mg). IR (KBr) ν: 3262, 3015, 1630, 1435, cm^{-1}. ^1H NMR (300 MHz, $CDCl_3$) δ: 8.44 (dt, $J1 = 5.8$ Hz, $J2 = 3.2$ Hz, 1H), 7.31-7-19 (m, 3H), 6.10 (t, $J = 5.0$ Hz, 1H), 4.10 (t, $J = 7.5$ Hz, 2H), 3.39 (td, $J1 = 5.5$ Hz, $J2 = 1.5$ Hz, 2H), 3.10 (t, $J = 6.8$ Hz, 2H), 2.60–2.40 (m, 6H), 2.38 (t, $J = 7.5$ Hz, 2H), 2.35 (s, 3H), 2.28–2.17 (m, 4H), 1.80 (quint, $J = 7.5$ Hz, 2H), 1.57 (quint, $J = 7.5$, 2H), 1.41 (quint, $J = 7.8$ Hz, 2H). ^{13}C NMR (101 MHz, $CDCl_3$) δ 169.1, 141.4, 136.2, 128.1, 122.6, 122.4, 121.5, 108.8, 107.1, 58.0, 54.6, 52.7, 45.7, 43.3, 41.4, 29.9, 27.3, 26.8, 26.4, 24.9. HRMS (ESI-MS) *m/z*: $[M+H]^+$ calcd for $C_{22}H_{33}N_4O$: 369.2649, found: 369.2653.

4.1.4. 2,3,4,5-Tetrahydro-6-(5-(4-methylpiperazin-1-yl)heptyl)azepino [4,3-b]indol-1(6H)-one (6b)

Compound **6a** was obtained as a brown oil, by starting from **4c** (380 mg, 1 mmol), anhydrous K_2CO_3 (415 mg, 3 mmol), and 1-methyl-piperazine (0.2 mL, 1.5 mmol). Yield: 61% (224 mg). IR (KBr) ν: 3260, 3017, 1628, 1432, cm^{-1}. ^1H NMR (300 MHz, $CDCl_3$) δ: 8.45 (t, $J = 5.8$ Hz, 1H), 7.30-7-20 (m, 3H), 6.10 (t, $J = 5.1$ Hz, 1H), 4.10 (t, $J = 7.3$ Hz, 2H), 3.39 (dd, $J1 = 10$ Hz, $J2 = 2.0$ Hz, 2H), 3.10 (t, $J = 7.0$ Hz, 2H), 2.70–2.50 (m, 6H), 2.36 (t, $J = 7.5$ Hz, 2H), 2.35 (s, 3H), 2.25–2.10 (m, 4H), 1.85–1.70 (m, 2H), 1.62–1.42 (m, 2H), 1.38–1.28 (m, 2H). ^{13}C NMR (101 MHz, $CDCl_3$) δ 169.0, 141.4, 136.2, 128.1, 122.7, 122.4, 121.4, 108.8, 107.1, 58.0, 54.6, 52.7, 45.7, 43.3, 41.4, 29.9, 27.3, 26.8, 26.4, 24.8. HRMS (ESI-MS) *m/z*: $[M+H]^+$ calcd for $C_{24}H_{37}N_4O$: 397.2962, found: 397.2967.

4.1.5. 2,3,4,5-Tetrahydro-6-[5-(4-phenylpiperazin-1-yl)pentyl]azepino [4,3-b]indol-1(6H)-one (7a)

Compound **7a** was obtained as a white solid, by starting from **4c** (350 mg, 1 mmol), anhydrous K_2CO_3 (415 mg, 3 mmol), and 1-phenyl-piperazine (0.23 mL, 1.5 mmol). Yield: 56% (241 mg). M.p. 185–186 °C. IR (KBr) ν: 3420, 3264, 3175, 3035, 2927, 2815, 1634, 1600, 1467, 1435, 1241, 1227, 996, 929, 799, 754, 691 cm^{-1}. 1H NMR (300 MHz, CDCl3) δ: 8.44 (dd, J1 = 7.0 Hz, J1 = 2.3 Hz, 1H), 7.33–7.18 (m, 5H), 6.92 (d, J = 8.5, 2H), 6.86 (t, $J = 6.9$ Hz, 1H), 5.96 (t, J = 5.3 H, 1H), 4.11 (t, $J = 7.5$ Hz, 2H), 3.37 (dd, J1 = 9.3 Hz, J2 = 4.7 Hz, 2H), 3.23–3.14 (m, 4H), 3.10 (t, $J = 6.7$ Hz, 2H), 2.60–2.52 (m, 4H), 2.41 (t, $J = 7.2$ Hz, 2H), 2.27–2.15 (m, 2H), 1.81 (quint, $J = 7.2$ Hz, 2H), 1.60–1.50 (m, 4H). ^{13}C NMR (101 MHz, $CDCl_3$) δ 168.9, 151.3, 141.3, 136.2, 129.1, 122.6, 122.4, 121.5, 119.8, 116.1, 108.8, 107.1, 57.7, 53.3, 49.2, 43.2, 41.5, 27.5, 27.3, 27.0, 24.2. HRMS (ESI-MS) *m/z*: $[M+H]^+$ calcd for $C_{27}H_{35}N_4O$: 431.2805, found: 431.2812. Anal $C_{27}H_{34}N_4O$ (C, H, N).

4.1.6. 2,3,4,5-Tetrahydro-6-{5-[4-(pyridin-2-yl)piperazin-1-yl]pentyl} azepino [4,3-b]indol-1(6H)-one (8a)

Compound **8a** was obtained as a yellow solid, by starting from **4c** (350 mg, 1 mmol), anhydrous K_2CO_3 (415 mg, 3 mmol), and 1-(2-Pyridyl)piperazine (250 mg, 1.5 mmol). Yield: 55% (237 mg). M.p. 159–162 °C. IR (KBr) ν: 3402, 3263, 3178, 3043, 2926, 1919, 1626, 1594, 1527, 1483, 1464, 1438, 1243, 774, 729 cm^{-1}. ^1H NMR (300 MHz, $CDCl_3$) δ: 8.43 (td, $J1 = 5.0$ Hz, $J2 = 1.5$ Hz, 1H), 8.19 (dd, $J1 = 4.9$ Hz, $J2 = 1.9$ Hz, 1H), 7.48 (dt, $J1 = 7.9$ Hz, $J2 = 1.9$ Hz, 1H), 7.36–7.16 (m, 3H), 6.63 (dd, $J1 = 10$ Hz, $J2 = 5.2$ Hz, 2H), 5.92 (t, $J = 5.3$ Hz, 1H), 4.09 (t, $J = 7.5$ Hz, 2H), 3.54 (t, $J = 5.0$, 4H), 3.38 (dd, $J = 9.3$ Hz, $J2 = 4.7$ Hz, 2H), 3.09 (t, $J = 6.7$ Hz, 2H), 2.53 (t, $J = 5.0$ Hz, 4H), 2.37 (t, $J = 7.5$ Hz, 2H), 2.28–2.15 (m, 2H), 1.79 (quint, $J = 7.7$ Hz, 2H), 1.57 (quint, $J = 7.8$ Hz, 2H), 1.44 (quint, $J = 8$ Hz, 2H). ^{13}C NMR (101 MHz, $CDCl_3$) δ 169.0, 159.6, 148.0, 141.3, 137.5, 136.2, 128.2, 122.6, 122.4, 121.4, 113.3, 108.8, 107.1, 58.7, 53.1, 45.2, 43.4, 41.5,

29.7, 29.3, 27.4, 27.3, 27.0, 26.9, 26.8. HRMS (ESI-MS) *m/z*: $[M+H]^+$ calcd for $C_{26}H_{34}N_5O$: 432.2758, found: 432.2762. Anal $C_{26}H_{33}N_5O$ (C, H, N).

*4.1.7. 2,3,4,5-Tetrahydro-6-{7-[4-(pyridin-2-yl)piperazin-1-yl]heptyl} azepino [4,3-b]indol-1(6H)-one (**8b**)*

Compound **8b** was obtained as a pale brown solid, by starting from **4d** (380 mg, 1 mmol), anhydrous K_2CO_3 (415 mg, 3 mmol), and 1-(2-Pyridyl)piperazine (250 mg, 1.5 mmol). Yield: 61% (280 mg). M.p. 141–143 °C. IR (KBr) *ν*: 3420, 3262, 3177, 3000, 2927, 1923, 1626, 1592, 1525, 1483, 1465, 1438, 1242, 773, 731 cm^{-1}. ^1H NMR (300 MHz, $CDCl_3$) δ: 8.43 (ddd, *J1* = 5.8 Hz, *J2* = 2.8 Hz, *J3* = 1.8 Hz, 1H), 8.18 (ddd, *J1* = 4.9 Hz, *J2* = 2.0 Hz, *J3* = 1.0 Hz, 1H), 7.48 (dt, *J1* = 9.0 Hz, *J2* = 2.0 Hz, 1H), 7.29–7.16 (m, 3H), 6.68–6.56 (m, 2H), 6.01 (t, *J* = 5.4 Hz, 1H), 4.06 (t, *J* = 7.6 Hz, 2H), 3.59–3.50 (m, 4H), 3.37 (ddd, *J1* = 8.4 Hz, *J2* = 5.5 Hz, *J3* = 1.5 Hz, 2H), 3.08 (t, *J* = 6.8, 2H), 2.56–2.50 (m, 4H), 2.39–2.31 (m, 2H), 2.27–2.16 (m, 2H), 1.74 (quint, *J* = 7.0 Hz, 2H), 1.52 (quint, *J* = 7.0 Hz, 2H), 1.44–1.29 (m, 6H). ^{13}C NMR (101 MHz, $CDCl_3$) δ 168.9, 159.6, 148.0, 141.3, 137.5, 136.2, 128.1, 122.6, 122.4, 121.5, 113.3, 108.7, 107.0, 58.5, 53.1, 45.2, 43.4, 41.5, 29.7, 27.3, 27.0, 26.6, 25.1. HRMS (ESI-MS) *m/z*: $[M+H]^+$ calcd for $C_{28}H_{38}N_5O$: 460.3071, found: 460.3073. Anal $C_{28}H_{38}N_5O$ (C, H, N).

*4.1.8. 6-{5-[4-(2-fluorophenyl)piperazin-1-yl]pentyl}-2,3,4,5-tetrahydroazepino[4,3-b]indol-1(6H)-one (**9a**)*

Compound **9a** was obtained as a white solid, by starting from **4c** (350 mg, 1 mmol), anhydrous K_2CO_3 (415 mg, 3 mmol), and 1-(2-Fluorophenyl)piperazine (0.2 mL, 1.5 mmol). Yield: 60% (270 mg). M.p. 250 °C-dec. IR (KBr) *ν*: 3430, 2844, 1909, 1869, 1552, 1434, 1205, 1002, 740, 726 cm^{-1}. ^1H NMR (300 MHz, $CDCl_3$) δ: 8.47–8.40 (m, 1H), 7.31–7.19 (m, 4H), 7.10–7.00 (m, 2H), 7.00–6.90 (m, 3H), 6.08 (t, *J* = 5.0 Hz, 1H), 4.07 (t, *J* = 7.7 Hz, 2H), 3.37 (dd, *J*1 = 9.5 Hz, *J*2 = 5.0 Hz, 2H), 3.11 (t, *J* = 5.4 Hz, 4H), 2.67–2.56 (m, 4H), 2.39 (t, *J* = 7.8 Hz, 2H), 2.28–2.17 (m, 2H), 1.81 (quint, *J* = 7.8 Hz, 2H), 1.57 (quint, *J* = 7.5, 2H), 1.41 (t, *J* = 7.5, 2H). HRMS (ESI-MS) *m/z*: $[M+H]^+$ calcd for $C_{27}H_{34}FN_4O$: 449.2711, found: 449.2717. Anal $C_{27}H_{33}FN_4O$ (C, H, N).

*4.1.9. 6-{7-[4-(2-fluorophenyl)piperazin-1-yl]heptyl}-2,3,4,5-tetrahydroazepino [4,3-b]indol-1(6H)-one (**9b**)*

Compound **9b** was obtained as a yellow solid, by starting from **4d** (380 mg, 1 mmol), anhydrous K_2CO_3 (415 mg, 3 mmol), and 1-(2-Fluorophenyl)piperazine (0.2 mL, 1.5 mmol). Yield: 59% (280 mg). M.p. 143–145 °C. IR (KBr) *ν*: 3413, 3263, 3177, 3038, 2927, 2855, 2820, 1923, 1890, 1805, 1772, 1627, 1502, 1464, 1440, 1238, 803, 751, 731, 686 cm^{-1}. ^1H NMR (300 MHz, $CDCl_3$) δ: 8.47–8.39 (m, 1H), 7.29–7.15 (m, 3H), 7.04 (qd, *J1* = 6.8 Hz, *J2* = 1.4 Hz, 2H), 6.94 (dt, *J1* = 8.7 Hz, *J2* = 4.4 Hz, 2H), 6.24 (br s, 1H), 4.05 (t, *J* = 7.7 Hz, 2H), 3.41–3.32 (m, 2H), 3.15–3.08 (m, 4H), 3.06 (t, *J* = 6.8 Hz, 2H), 2.66–2.57 (m, 4H), 2.38 (t, *J* = 7.8 Hz, 2H), 2.26–2.15 (m, 2H), 1.75 (quint, *J* = 7.2 Hz, 2H), 1.51 (quint, *J* = 7.4 Hz, 2H), 1.43–1.29 (m, 6H). ^{13}C NMR (101 MHz, $CDCl_3$) δ 169.1, 155.9 (d, *J* = 245.7 Hz), 141.5, 140.3 (d, *J* = 8.4 Hz), 136.4, 128.3, 124.6 (d, *J* = 3.5 Hz), 122.7, 122.6 (d, *J* = 9.3 Hz), 122.5, 121.6, 119.1 (d, *J* = 3.1 Hz), 116.2 (d, *J* = 20.8 Hz), 108.9, 107.2, 58.8, 53.5, 50.7, 43.6, 41.7, 29.9, 29.5, 27.6, 27.4, 27.2, 27.1, 26.9. HRMS (ESI-MS) *m/z*: $[M+H]^+$ calcd for $C_{29}H_{38}FN_4O$: 477.3024, found: 477.3032. Anal $C_{29}H_{37}FN_4O$ (C, H, N).

*4.1.10. 6-{5-[4-(4-fluorophenyl)piperazin-1-yl]pentyl}-2,3,4,5-tetrahydroazepino [4,3-b]indol-1(6H)-one (**10a**)*

Compound **10a** was obtained as a white solid, by starting from **4c** (350 mg, 1 mmol), anhydrous K_2CO_3 (415 mg, 3 mmol), and 1-(4-Fluorophenyl)piperazine (290 mg, 1.5 mmol). Yield: 60% (270 mg). M.p. 156–159 °C. IR (KBr) *ν*: 1628, 1515, 1485, 1462, 1384, 1224, 820, 746 cm^{-1}. ^1H NMR (300 MHz, $CDCl_3$) δ: 8.44 (td, *J1* = 4.7 Hz, *J2* = 1.3 Hz, 1H), 7.28–7.18 (m, 3H), 6.95 (t, *J* = 8.0 Hz, 2H), 6.86 (dd, *J1* = 10.0 Hz, *J2* = 5.2 Hz, 2H), 5.97 (t, *J* = 5.4 Hz, 1H), 4.08 (t, *J* = 7.6 Hz, 2H), 3.37 (dd, *J1* = 8.4 Hz, *J2* = 5.5 Hz, 2H), 3.15–3.04 (m, 6H), 2.61–2.53 (m, 4H), 2.37 (t, *J* = 7.7 Hz, 2H), 2.28–2.14 (m, 2H), 1.79 (quint, *J* = 7.6, 2H), 1.57 (quint, *J* = 8.0 Hz, 2H), 1.43 (quint, *J* = 7.5 Hz, 2H). ^{13}C NMR (101 MHz, $CDCl_3$) δ 169.1, 157.3 (d, *J* = 238.9 Hz), 148.1 (d, *J* = 2.2 Hz), 141.4, 136.4, 128.3, 122.8, 122.5, 121.6, 117.9 (d, *J* = 7.6 Hz), 115.7 (d, *J* = 22.1 Hz), 108.9, 107.3, 58.5, 53.5, 503, 43.5, 41.6, 29.8, 27.4, 27.2, 26.8, 25.2. HRMS (ESI-MS) *m/z*: $[M+H]^+$ calcd for $C_{27}H_{34}FN_4O$: 449.2711, found: 449.2716. Anal $C_{27}H_{33}FN_4O$ (C, H, N).

*4.1.11. 6-{7-[4-(4-fluorophenyl)piperazin-1-yl]heptyl}-2,3,4,5-tetrahydroazepino [4,3-b]indol-1(6H)-one (**10b**)*

Compound **10b** was obtained as a pale yellow solid, by starting from **4d** (380 mg, 1 mmol), anhydrous K_2CO_3 (415 mg, 3 mmol), and 1-(4-Fluorophenyl)piperazine (290 mg, 1.5 mmol). Yield: 42% (200 mg). M.p. 146–147 °C. IR (KBr) *ν*: 3262, 3033, 2925, 2855, 1625, 1380, 1224, 820, 730 cm^{-1}. ^1H NMR (300 MHz, $CDCl_3$) δ: 8.46 (d, *J* = 5.0 Hz 1H), 7.25–7.18 (m, 3H), 6.98 (t, *J* = 8.0 Hz, 2H), 6.90 (dd, *J1* = 10.0 Hz, *J2* = 5.2 Hz, 2H), 5.97 (t, *J* = 5.5 Hz, 1H), 4.10 (t, *J* = 8.0 Hz, 2H), 3.37 (dd, *J1* = 8.4 Hz, *J2* = 5.5 Hz, 2H), 3.30–3.05 (m, 6H), 2.60–2.50 (m, 4H), 2.37 (t, *J* = 7.7 Hz, 2H), 2.30–2.20 (m, 2H), 1.80–1.73 (m, 4H), 1.54 (quint, *J* = 6.0 Hz, 2H), 1.52–1.40 (m, 6H). ^{13}C NMR (101 MHz, $CDCl_3$) δ 169.0, 157.1 (d, *J* = 239.0 Hz), 148.0 (d, *J* = 2.1 Hz), 141.2, 136.2, 128.4, 122.9, 122.5, 121.5, 118.0 (d, *J* = 7.7 Hz), 115.8 (d, *J* = 22.0 Hz), 108.7, 107.3, 58.5, 53.5, 503, 43.5, 41.6, 29.8, 27.4, 27.2, 26.8, 25.2. HRMS (ESI-MS) *m/z*: $[M+H]^+$ calcd for $C_{27}H_{34}FN_4O$: 449.2711, found: 449.2718. Anal $C_{27}H_{33}FN_4O$ (C, H, N).

*4.1.12. 6-[2-(4-benzylpiperazin-1-yl)ethyl]-2,3,4,5-tetrahydroazepino [4,3-b]indol-1(6H)-one (**11a**)*

Compound **11a** was obtained as a yellow solid, by starting from **4a** (310 mg, 1 mmol), anhydrous K_2CO_3 (415 mg, 3 mmol), and 1-(benzyl) piperazine (265 mg, 1.5 mmol). Yield: 50% (202 mg). M.p. 143–145 °C. IR (KBr) *ν*: 3401, 3263, 2926, 2806, 1628, 1525, 1464, 1159, 745, 736, 695 cm^{-1}. ^1H NMR (300 MHz, $CDCl_3$) δ 8.46–8.42 (m, 1H), 7.42–7.19 (m, 8H) 5.98–5.85 (m, 1H), 4.20 (t, *J* = 7.2 Hz, 2H), 3.52 (s, 2H), 3.37 (dd, *J1* = 8.6, *J2* = 4.4 Hz, 2H), 3.14 (t, *J* = 6.8 Hz, 2H), 2.66 (t, *J* = 7.1 Hz, 2H), 2.55 (s, 4H), 2.49 (s, 4H), 2.21 (dd, *J1* = 16.2, *J2* = 7.8 Hz, 2H). ^{13}C NMR (101 MHz, $CDCl_3$) δ 169.1, 141.9, 137.8, 136.3, 129.4, 128.4, 128.4, 127.4, 122.8, 122.62 (s), 121.7, 108.7, 107.3, 63.0, 57.1, 53.7, 53.1, 41.6, 41.6 27.6 (s), 27.0. HRMS (ESI-MS) *m/z*: $[M+H]^+$ calcd for $C_{25}H_{31}N_4O$: 403.2492, found: 403.2488. Anal $C_{25}H_{30}N_4O$ (C, H, N).

*4.1.13. 6-[4-(4-benzylpiperazin-1-yl)butyl]-2,3,4,5-tetrahydroazepino [4,3-b]indol-1(6H)-one (**11b**).*

Compound **11b** was obtained as a pale brown solid, by starting from **4b** (335 mg, 1 mmol), anhydrous K_2CO_3 (415 mg, 3 mmol), and 1-(benzyl)piperazine (265 mg, 1.5 mmol). Yield: 56% (242 mg). M.p. 113–115 °C. IR (KBr) *ν*: 3435, 2934, 2826, 1642, 1604, 1459, 1153, 750 cm^{-1}. ^1H NMR (300 MHz, $CDCl_3$) δ: 8.45–8.38 (m, 1H), 7.35–7.25 (m, 4H), 7.28–7.18 (m, 4H), 6.00 (t, *J* = 5.0 Hz, 1H), 4.10 (d, *J* = 7.6 Hz, 1H), 4.07 (d, *J* = 7.6 Hz, 1H), 3,51 (s, 2H), 3.36 (dd, *J1* = 9.8 Hz, *J2* = 5.3 Hz, 2H), 3.08 (t, *J* = 6.7 Hz, 2H), 2.55–2.40 (m, 8H), 2.35 (t, *J* = 7.4 Hz, 2H), 2.20 (dd, *J1* = 16 Hz, *J2* = 6.7 Hz, 2H), 1.82–1.69 (m, 2H), 1.57 (quint, *J* = 7.4 Hz, 2H). ^{13}C NMR (101 MHz, CDCl3) δ 169.0, 141.3, 138.0, 136.2, 129.2, 128.2, 128.2, 127.1, 122.6, 122.4, 121.4, 108.8, 107.1, 63.1, 57.7, 53.2, 53.1, 43.2, 41.5, 27.6, 27.3, 26.9, 24.2. HRMS (ESI-MS) *m/z*: $[M+H]^+$ calcd for $C_{27}H_{35}N_4O$: 431.2805, found: 431.2812. Anal $C_{27}H_{34}N_4O$ (C, H, N).

*4.1.14. 6-[5-(4-benzylpiperazin-1-yl)pentyl]-2,3,4,5-tetrahydroazepino [4,3-b]indol-1(6H)-one (**11c**)*

Compound **11c** was obtained as a yellow solid, by starting from **4c** (350 mg, 1 mmol), anhydrous K_2CO_3 (415 mg, 3 mmol), and 1-(benzyl) piperazine (265 mg, 1.5 mmol). Yield: 50% (223 mg). M.p. 118–120 °C. IR (KBr) *ν*: 3434, 3266, 3042, 2929, 2862, 2806, 1626, 1485, 1159, 1016, 743 cm^{-1}. ^1H NMR (300 MHz, $CDCl_3$) δ: 8.45–8.37 (m, 1H),

7.36–7.28 (m, 4H), 7.25–7.18 (m, 4H), 5.91 (t, $J = 5$ Hz, 1H), 4.07 (t, $J = 7.6$ Hz, 2H), 3.50 (s, 2H), 3.37 (dd, $J1 = 9.9$ Hz, $J2 = 5.3$ Hz, 2H), 3.08 (t, $J = 6.7$ Hz, 2H), 2.60–2.38 (m, 8H). 2.31 (t, $J = 7.8$ Hz, 2H), 2.26–2.14 (m, 2H), 1.77 (quint, $J = 7.7$ Hz, 2H), 1.52 (quint, $J = 7.6$ Hz, 2H), 1.40 (quint, $J = 7.8$, 2H). ^{13}C NMR (101 MHz, CDCl3) δ 169.0, 141.3, 138.0, 136.2, 129.3, 128.2, 127.1, 122.6, 122.4, 121.4, 198.8, 107.1, 64.0, 58.4, 53.3, 53.0, 43.4, 41.5, 29.6, 27.3, 27.0, 26.5, 25.1. HRMS (ESI-MS) *m/z*: $[M+H]^+$ calcd for $C_{28}H_{37}N_4O$: 445.2962, found: 445.2966. Anal $C_{28}H_{36}N_4O$ (C, H, N).

*4.1.15. 6-[7-(4-benzylpiperazin-1-yl)heptyl]-2,3,4,5-tetrahydroazepino [4,3-b]indol-1(6H)-one (**11d**)*

Compound **11d** was obtained as a white solid, by starting from **4d** (380 mg, 1 mmol), anhydrous K_2CO_3 (415 mg, 3 mmol), and 1-(benzyl) piperazine (265 mg, 1.5 mmol). Yield: 63% (297 mg). M.p. 138–140 °C. IR (KBr) *ν*: 3398, 3263, 3178, 3034, 2927, 2856, 2808, 2770, 1626, 1463, 1156, 798, 731 cm^{-1}. ^{1}H NMR (300 MHz, $CDCl_3$) δ: 8.43 (dd, *J1* = 6.2 Hz, *J2* = 2.9 Hz, 1H), 7.31 (d, $J = 4.4$ Hz, 3H), 7.27–7.20 (m, 5H), 5.93 (t, $J = 5.2$ Hz, 1H), 4.06 (t, $J = 7.5$ Hz, 2H), 3.51 (s, 2H), 3.41–3.34 (m, 2H), 3.08 (t, $J = 6.8$ Hz, 2H), 2.62–2.37 (m, 8H), 2.30 (t, $J = 7.9$ Hz, 2H), 2.25–2.18 (m, 2H), 1.74 (quint, $J = 7.5$ Hz, 2H), 1.46 (quint, $J = 7.7$ Hz, 2H), 1.41–1.25 (m, 6H). ^{13}C NMR (101 MHz, CDCl3) δ 169.0, 141.4, 138.1, 136.2, 129.2, 128.2, 127.0, 122.6, 122.3, 121.4, 108.8, 107.0, 63.1, 58.6, 53.2, 53.0, 43.4, 41.5, 29.7, 29.3, 27.4, 27.3, 27.0, 26.9, 26.8. HRMS (ESI-MS) *m/z*: $[M+H]^+$ calcd for $C_{30}H_{41}N_4O$: 473.3275, found: 473.3297. Anal $C_{30}H_{40}N_4O$ (C, H, N).

*4.1.16. 2,3,4,5-Tetrahydro-6-{5-{4-[(pyridin-3-yl)methyl]piperazin-1-yl} pentyl}azepino [4,3-b]indol-1(6H)-one (**12a**)*

Compound **12a** was obtained as a yellow wax solid, by starting from **4c** (350 mg, 1 mmol), anhydrous K_2CO_3 (415 mg, 3 mmol), and 1-((pyridin-3-yl)methyl)piperazine hydrochloride (330 mg, 1.5 mmol). Yield: 48% (215 mg). IR (KBr) *ν*: 3264, 3032, 2938, 2765, 1625, 1462, 1440, 1160, 800, 729 cm^{-1}. ^{1}H NMR (300 MHz, $CDCl_3$) δ: 8.54 (d, $J = 1.7$ Hz, 1H), 8.50 (dd, *J1* = 4.8 Hz, *J2* = 1.6 Hz, 1H), 8.43 (dd, *J1* = 7.2 Hz, *J2* = 1.8 Hz, 1H), 7.65 (dt, *J1* = 7.8 Hz, *J2* = 1.8 Hz, 1H), 7.25–7.20 (m, 4H), 5.91 (t, $J = 5.2$ Hz, 1 H), 4.07 (m, 2H), 3.51 (s, 2H), 3.37 (dt, *J1* = 5.4 Hz, *J2* = 1.5 Hz, 2H), 3.08 (t, $J = 6.8$ Hz, 2H), 2.48 (br s, 8H), 2.33 (m, 2H), 2.22 (dt, *J1* = 8.3 Hz, *J2* = 6.7 Hz, 2H), 1.77 (quint, $J = 7.5$ Hz, 2H), 1.53 (quint, $J = 7.5$ Hz, 2H). ^{13}C NMR (101 MHz, $CDCl_3$) δ 169.2, 150.6, 148.8, 141.5, 136.9, 136.3, 133.6, 128.3, 123.4, 122.7, 122.5, 121.6, 108.9, 107.2, 60.3, 59.0, 58.3, 53.2, 52.9, 43.5, 41.6, 29.7, 27.4, 27.1, 26.5, 25.1, 24.1, 19.9, 13.8. HRMS (ESI-MS) *m/z*: $[M+Na]^+$ calcd for $C_{27}H_{35}N_5Ona$: 468.2734, found: 468.2733.

*4.1.17. 2,3,4,5-Tetrahydro-6-{7-{4-[(pyridin-3-yl)methyl]piperazin-1-yl} heptyl}azepino [4,3-b]indol-1(6H)-one (**12b**)*

Compound **12b** was obtained as a brown oil, by starting from **4d** (380 mg, 1 mmol), anhydrous K_2CO_3 (415 mg, 3 mmol), and 1-((pyridin-3-yl)methyl)piperazine hydrochloride (330 mg, 1.5 mmol). Yield: 49% (230 mg). IR (KBr) *ν*: 3262, 3030, 2935, 1627, 802, 727 cm^{-1}. ^{1}H NMR (300 MHz, $CDCl_3$) δ: 8.54 (d, $J = 1.6$ Hz, 1H), 8.50 (dd, *J*1 = 4.8 Hz, *J*2 = 1.6 Hz, 1H), 8.43 (m, 1H), 7.65 (dt, *J*1 = 7.9 Hz, 2.0 Hz, 1H), 7.25–7.18 (m, 4H), 5.96 (t, $J = 5.4$ Hz, 1H), 4.06 (m, 2H), 3.51 (s, 2H), 3.37 (dt, *J*1 = 5.5 Hz, *J*2 = 1.5 Hz, 2H), 3.08 (t, $J = 6.8$ Hz, 2H), 2.48 (br s, 8H), 2.31 (m, 2H), 2.22 (dt, *J*1 = 8.4 Hz, *J*2 = 6.7 Hz, 2H), 1.51–1.23 (m, 10H). HRMS (ESI-MS) *m/z*: $[M+Na]^+$ calcd for $C_{29}H_{39}N_5ONa$: 496.3047, found: 496.3058.

*4.1.18. 2,3,4,5-Tetrahydro-6-{5-{4-[(pyridin-4-yl)methyl]piperazin-1-yl} pentyl}azepino [4,3-b]indol-1(6H)-one (**13a**)*

Compound **13a** was obtained as a yellow amorphous solid, by starting from **4c** (350 mg, 1 mmol), anhydrous K_2CO_3 (415 mg, 3 mmol), and 1-((pyridin-4-yl)methyl)piperazine hydrochloride (330 mg, 1.5 mmol). Yield: 43% (191 mg). IR (KBr) *ν*: 3263, 3179, 2940, 2802, 1626, 1463, 1440, 1163, 834, 728 cm^{-1}. ^{1}H NMR (300 MHz, $CDCl_3$) δ: 8.53 (dd, *J1* = 4.4 Hz, *J2* = 1.5 Hz, 2H), 8.43 (dd, *J1* = 6.1 Hz, *J2* = 2.9 Hz, 1H), 7.29–7.18 (m, 5H), 5.93 (t, $J = 5.6$ Hz, 1H), 4.08, (t, $J = 7.6$ Hz, 2H), 3.50 (s, 2H), 3.37 (dt, *J1* = 10.1 Hz, *J2* = 5.4 Hz, 2H), 3.08 (t, $J = 6.1$ Hz, 2H), 2.46 (br s, 8H), 2.31 (m, 2H), 2.22–2.10 (m, 2H), 1.78 (m, 2H), 1.56 (m, 2H), 1.42 (m, 2H). ^{13}C NMR (101 MHz, $CDCl_3$) δ 169.1, 149.9, 147.6, 141.4, 136.3, 128.3, 124.0, 122.8, 122.5, 121.6, 108.9, 107.3, 61.8, 58.4, 53.3, 53.2, 43.5, 41.6, 29.7, 27.4, 27.1, 26.6, 25.2. HRMS (ESI-MS) *m/z*: $[M+Na]^+$ calcd for $C_{27}H_{35}N_5Ona$: 468.2734, found: 468.2732.

*4.1.19. 2,3,4,5-Tetrahydro-6-{7-{4-[(pyridin-4-yl)methyl]piperazin-1-yl} heptyl}azepino [4,3-b]indol-1(6H)-one (**13b**)*

Compound **13b** was obtained as a yellow oil, by starting from **4d** (380 mg, 1 mmol), anhydrous K_2CO_3 (415 mg, 3 mmol), and 1-((pyridin-4-yl)methyl)piperazine hydrochloride (330 mg, 1.5 mmol). Yield: 57% (270 mg). IR (KBr) *ν*: 3264, 3038, 2928, 2343, 2298, 1926, 1626, 1464, 1440, 1158, 803, 732 cm^{-1}. ^{1}H NMR (300 MHz, $CDCl_3$) δ: 8.52 (d, $J = 5.9$ Hz, 2H), 8.42 (dd, *J*1 = 6.3 Hz, *J*2 = 2.4 Hz, 1H), 7.18–7.29 (m, 5H), 5.98 (t, $J = 5.3$ Hz, 1H), 4.06 (m, 2H), 3.50 (s, 2H), 3.36 (t, $J = 4.2$ Hz, 2H), 3.08 (t, $J = 6.8$ Hz, 2H), 2.49 (br s, 8H), 2.33 (m, 2H), 2.21 (dt, *J*1 = 7.1 Hz, *J*2 = 6.3 Hz, 2H), 1.74 (dt, *J*1 = 15.6 Hz, *J*2 = 7.8 Hz, 2H), 1.68 (dt, *J*1 = 15.8 Hz, *J*2 = 7.8 Hz, 2H), 1.58–1.41 (m, 6H). ^{13}C NMR (101 MHz, $CDCl_3$) δ 169.2, 149.9, 147.6, 141.5, 136.4, 128.3, 124.0, 122.7, 122.5, 121.6, 108.9, 107.2, 61.8, 58.6, 53.2, 52.9, 43.6, 41.6, 29.8, 29.4, 27.5, 27.4, 27.1, 24.3, 19.9, 13.8. HRMS (ESI-MS) *m/z*: $[M+Na]^+$ calcd for $C_{29}H_{39}N_5ONa$: 496.3047, found: 496.3056.

*4.1.20. 6-[2-(4-phenethylpiperazin-1-yl)ethyl]-2,3,4,5-tetrahydroazepino [4,3-b]indol-1(6H)-one (**14a**)*

Compound **14a** was obtained as a yellow solid, by starting from **4a** (310 mg, 1 mmol), anhydrous K_2CO_3 (415 mg, 3 mmol), and 1-(phenylethyl)piperazine (285 mg, 1.5 mmol). Yield: 53% (220 mg). M.p. 165–166 °C. IR (KBr) *ν*: 3412, 3315, 3049, 2948, 2929, 2829, 1901, 1625, 1529, 1463, 1148, 1128, 751 cm^{-1}. ^{1}H NMR (300 MHz, $CDCl_3$) δ 8.44 (d, $J = 9.0$ Hz, 1H), 7.32–7.25 (m, 4H), 7.23–7.18 (m, 4H), 5.88 (t, $J = 5.0$ Hz, 1H), 4.22 (t, $J = 7.2$ Hz, 2H), 3.38 (dd, *J1* = 9.2, *J1* = 5.5 Hz, 2H), 3.16 (t, $J = 7.0$ Hz, 2H), 2.79 (dd, *J1* = 10.0, *J1* = 6.0 Hz, 2H), 2.69 (t, $J = 7.2$ Hz, 2H), 2.62–2.50 (m, 10H), 2.30–2.18 (m, 2H). ^{13}C NMR (101 MHz, $CDCl_3$) δ 168.9, 141.8, 140.2, 126.7, 126.6, 126.1, 122.7, 122.5, 121.6, 108.6, 107.2, 60.4, 57.0, 53.7, 53.2, 41.5, 41.4, 33.6, 27.5, 26.9. HRMS (ESI-MS) *m/z*: $[M+H]^+$ calcd for $C_{26}H_{33}N_4O$: 417.2649, found: 417.2651. Anal $C_{26}H_{32}N_4O$ (C, H, N).

*4.1.21. 6-[4-(4-phenethylpiperazin-1-yl)butyl]-2,3,4,5-tetrahydroazepino [4,3-b]indol-1(6H)-one (**14b**)*

Compound **14b** was obtained as a yellow solid, by starting from **4b** (330 mg, 1 mmol), anhydrous K_2CO_3 (415 mg, 3 mmol), and 1-(phenylethyl)piperazine (285 mg, 1.5 mmol). Yield: 48% (213 mg). M.p. 150–152 °C. IR (KBr) *ν*: 3435, 3030, 2944, 2821, 1636, 1522, 1462, 1384, 1129, 751 cm^{-1}.^{1}H NMR (300 MHz, $CDCl_3$) δ: 8.43 (dd, *J1* = 8.9 Hz, *J2* = 2.0 Hz, 1H), 7.30–7.19 (m, 8H), 5.98 (t, $J = 4.8$ Hz, 1H), 4.12 (dd, *J1* = 15 Hz, *J2* = 7.1 Hz, 2H), 3.37 (dd, *J1* = 9.0 Hz, *J2* = 4.7 Hz), 3.09 (t, $J = 6.7$ Hz, 2H), 2.85–2.72 (m, 2H), 2.68–2.43 (m, 10H), 2.38 (t, $J = 7.2$ Hz, 2H), 2.27–2.12 (m, 2H), 1.79 (quint, $J = 7.2$ Hz, 2H), 1.59 (quint, $J = 7.3$ Hz, 2H). ^{13}C NMR (101 MHz, $CDCl_3$) δ 169.0, 141.3, 140.3, 136.2, 128.7, 128.4, 128.2, 126.1, 122.6, 122.4, 121.5, 108.8, 107.1, 60.5, 57.7, 53.2, 43.2, 41.5, 33.6, 27.6, 27.3, 27.0, 24.2. HRMS (ESI-MS) *m/z*: $[M+H]^+$ calcd for $C_{28}H_{37}N_4O$: 445.2962, found: 445.2968. Anal $C_{28}H_{36}N_4O$ (C, H, N).

*4.1.22. 6-[5-(4-phenethylpiperazin-1-yl)pentyl]-2,3,4,5-tetrahydroazepino [4,3-b]indol-1(6H)-one (**14c**)*

Compound **14c** was obtained as a white solid, by starting from **4c** (350 mg, 1 mmol), anhydrous K_2CO_3 (415 mg, 3 mmol), and 1-(phenylethyl)piperazine (285 mg, 1.5 mmol). Yield: 53% (243 mg). M.p. 143–146 °C. IR (KBr) *ν*: 3436, 3265, 3180, 3030, 2929, 2806, 1626,

1526, 1463, 1159, 1135, 728, 700 cm^{-1}. ^1H NMR (300 MHz, $CDCl_3$) δ: 8.43 (dd, *J1* = 8.7 Hz, *J2* = 2.0 Hz, 1H), 7.36–7.13 (m, 8H), 5.93 (t, *J* = 5.1 Hz, 1H), 4.08 (t, *J* = 7.6 Hz, 2H), 3.37 (dd, *J1* = 9.8 Hz, *J2* = 5.3 Hz, 2H), 3.08 (t, *J* = 6.7 Hz, 2H), 2.85–2.72 (m, 2H), 2.66–2.40 (m, 10 H), 2.33 (t, *J* = 7.8 Hz, 2H), 2.27–2.14 (m, 2H), 1.77 (quint, *J* = 7.5 Hz, 2H), 1.55 (quint, *J* = 7.5 Hz, 2H), 1.40 (quint, *J* = 7.5 Hz, 2H). ^{13}C NMR (101 MHz, $CDCl_3$) δ 169.0, 141.3, 140.3, 136.2, 128.7, 128.6, 126.1, 122.6, 122.4, 121.5, 108.7, 60.5, 58.4, 53.3, 53.2, 43.4, 41.5, 33.6, 29.6, 27.3, 27.0, 26.6, 25.0. HRMS (ESI-MS) *m/z*: $[M+H]^+$ calcd for $C_{29}H_{39}N_4O$: 459.3118, found: 459.3121. Anal $C_{29}H_{38}N_4O$ (C, H, N).

4.1.23. 6-(7-(4-4-phenethylpiperazin-1-yl)heptyl)-2,3,4,5-tetrahydroazepino [4,3-b]indol-1(6H)-one (**14d**)

Compound **14d** was obtained as a white solid, by starting from **4d** (380 mg, 1 mmol), anhydrous K_2CO_3 (415 mg, 3 mmol), and 1-(phenylethyl)piperazine (285 mg, 1.5 mmol). Yield: 59% (287 mg). M.p. 151–154 °C. IR (KBr) *ν*: 3436, 3263, 3178, 3029, 2928, 2859, 2810, 2771,1626, 1525, 1464, 1440, 1179, 1159, 1129, 745, 731 cm^{-1}. ^1H NMR (300 MHz, $CDCl_3$) δ: 8.47–8.40 (m, 1H), 7.31–7.23 (m, 4H), 7.21–7.17 (m, 4H), 7.21–7.17 (m, 4H), 5.90 (t, *J* = 5.3 Hz, 1H), 4.07 (dd, *J1* = 14 Hz, *J2* = 6.5 Hz, 2H), 3.37 (dd, *J1* = 10 Hz, *J2* = 5.4 Hz, 2H), 3.08 (t, *J* = 6.8 Hz, 2H), 2.80 (dd, *J1* = 10 Hz, *J2* = 5.7 Hz, 2H), 2.67–2.37 (m, 10H), 2.37–2.27 (m, 2H), 2.22 (dt, *J1* = 8.4 Hz, *J2* = 6.8 Hz, 2H), 1.74 (quint, *J* = 7.5 Hz, 2H), 1.48 (quint, *J* = 7.5 Hz, 2H), 1.40–1.28 (m, 6H). ^{13}C NMR (101 MHz, $CDCl_3$) δ 168.9, 141.3, 140.3, 136.2, 128.7, 128.4, 126.0, 122.5, 122.3, 121.4, 108.8, 107.0, 60.5, 58.7, 53.3, 53.1, 43.4, 41.4, 33.6, 29.7, 29.3, 27.4, 27.3, 27.0, 26.9, 26.7. HRMS (ESI-MS) *m/z*: $[M+H]^+$ calcd for $C_{31}H_{43}N_4O$: 487.3431, found: 487.3428. Anal $C_{31}H_{43}N_4O$ (C, H, N).

4.2. Molecular modelling

The SMILES string of ligands was converted to three-dimensional structure within Open Babel [60] software package assigning the ionization state with *fixpka* complement of QUACPAC [61]. The molecular skeleton was relaxed performing 10000 steps of Steepest Descent minimization by using the Universal Force Field and the *molcharge* complement of QUACPAC was used to achieve Marsili-Gasteiger charges. Dockings were carried out on selected targets namely the BChE/TKN enzyme-inhibitor complexes (entry 7BGC in the Protein Brookhaven Database) [62]. The X-ray structures were prepared with the Protein Preparation Wizard interface of Maestro [63] removing the co-crystallized ligand and water molecules, completing the whole structure with hydrogen atoms, then optimizing their position, and assigning the ionization states of acid and basic residues according to PROPKA prediction at pH 7.0. For protein atoms electrostatic charges were loaded according to AMBER UNITED force field [64] A 0.375 Å spaced boxes 60 × 110 × 50 Å, having the barycentre on the co-crystallized cognate ligand, was considered for affinity maps calculations, and the binding site available space was screened throughout 1000 runs of Lamarckian Genetic Algorithm (LGA) implemented in AUTODOCK 4.2.6 [65] using the GPU-OpenCL algorithm version [66]. Water molecules contribution in the binding was achieved with the hydration force field parameters [67], and the population size and the number of energy evaluation figures were set to 300 and 10000000, respectively. Docking poses were ranked by **ESP**, a simple energy-, similarity- and population-based rule, proved to be efficient in similar structure-based studies focused on esterases ligands.[68,69] In this metric **E** accounts for the free energy of binding, the energy difference between the selected pose and the relative global minimum and the ligand efficacy, **S** the similarity as scored by the Tanimoto-Combo coefficient according to the shape matching algorithm ROCS [70], **P** is the cluster member population. The rule was applied as a cut-off threshold, judging valuable a pose only if endows a lone violation of the same rule parameters as following: **FEB** < -8.00, **ΔE** < 2.00, **EFF** < -0.200, **TAN** > 0.700, **POP** $> 10/1000$.

4.3. Surface plasmon resonance assays

4.3.1. Kinetics of interactions with equine BChE

Affinity studies by using surface plasmon resonance were performed on a Pioneer SensiQ SPR instrument (Pall FortèBio, Alfatest, Cinisello Balsamo, Milan, Italy). BChE was first immobilized on a COOH V sensor chip (Pall FortèBio) surface by amine coupling, resulting in a stable biosensor. After purification and conditioning of the new sensor chip by flowing HCl, NaOH, and SDS, the surface underwent equilibration by flowing 10 mM phosphate buffer (pH 8) at a flow rate of 20 μL/min. The carboxymethylated dextran layer on the sensor chip surface was then activated within 10 min by injection of an EDC/NHS. Equine BChE (50 U/mL) was dissolved in 10 mM mM sodium acetate (pH 4.5) and coupled over surface by three different and sequential injection of enzyme solutions for 10 min at a flow rate of 25 μL/min. After immobilization of the ligand, the unreacted NHS esters were blocked by washing overnight (throughout 18 h) with 0.05 M TRIS solution (pH 8), containing 0.1 M NaCl, at a flow rate of 20 μL/min. Stability of the biosensors was tested by repeating regeneration cycles with a 3 M NaCl solution injection (5 μL, flow 50 μL/min), without any significant change in the surface responses. Immobilization of the BChE was obtained in flow cells 1 and 3 (unmodified dextran surface in flow cell 2 was used as a reference). A final apparent level of about 6500–6750 RU was achieved. The assay protocol was the follow. Assay solutions of tested compounds were prepared by dissolving 10 mM DMSO solutions in 10 mM phosphate buffer (pH 8) up to a final 2% DMSO concentration, as in the running buffer. After 10 leadoff blanks, the assay solutions were injected over BChE functionalized surface 4 min at a flow rate of 25 μL/min, to avoid any limitation by mass transfer. On completion of injection, the running buffer flowed to allow a dissociation time of 180 s. All binding experiments were carried out at 25 °C, without regeneration cycles were necessary. Each interaction was repeated at least in triplicate and analyzed by using QDAT software (non-linear regression analysis of 1:1 stoichiometric reversible binding model), and double referencing.

4.3.2. Kinetics of interactions with human serum albumin (HSA)

The HSA functionalized surface on COOH V sensor chip (Pall FortèBio) was prepared by using amine coupling (EDC/NHS) and HSA (Sigma-Aldrich A3782) [38]. Briefly, HSA aqueous stock solution was diluted at the final concentration of 50 μg/mL in 10 mM sodium acetate buffer (pH 5.0), and immobilization in flow cells 1 and 3 (unmodified dextran surface in flow cell 2 was used as a reference) at a final apparent level of about 5000 RU was achieved as followed: injection of EDC/NHS (freshly mixed 0.4 M EDC and 0.1 M NHS) 1:1v/v at flow 25 μL/min1 for 4 min; injection of HSA solution at flow 25 μL/min1 for 8 min; capping on unreacted activated carboxyl groups by injection of 1 M ethanolamine solution (pH 9) at flow 25 μL/min for 8 min. Functionalized surface was then treated with repeated injection of 4 M NaCl, and conditioned overnight prior to use with pH 7.4 PBS (10 mM NaH_2PO_4 and 150 mM NaCl) as running buffer. Each cycle, without regeneration necessary, for binding assay to HSA was carried out in PBS-2% DMSO and consisted of run buffer injection (60 s), injection of analyte single concentration for 120 s (ranging from 1 to 200 μM) at a flow 20 μL/min, and dissociation phase for 150 s (flow 20 μL/min). Each interaction was performed at least in triplicate and analyzed by using QDAT software (non-linear regression analysis of 1:1 stoichiometric reversible binding model), and double referencing.

4.4. Biological assays

4.4.1. Cholinesterases inhibition

The inhibitory activity of new synthesized compounds toward horse and human BChE and either electric eel AChE (Sigma-Aldrich), was assessed by following the Ellman's method, with slight modifications, on a 96-wells plate system.[71,72] The BChE activity was determined in a

reaction mixture containing 20 μL of a BChE solution (1.8 U/mL in 0.1 M pH 8.0 phosphate buffer, PB), 20 μL of 5,5-dithio-bis-(2-nitrobenzoic) acid (DTNB 3.3 mM in 0.1 M pH 7.0 PB, containing 0.1 mM $NaHCO_3$), 20 μL of a solution of the test compound (ranging from 1×10^{-4} to 1×10^{-9} M in 0.1 M pH 8.0 PB), and 120 μL of pH 8.0 PB. After 20 min incubation at 25 °C, the substrate butyrylthiocholine iodide (20 μL, 0.05 mM solution in PB) was added, and its hydrolysis rate was monitored for 10 min at 412 nm. The concentration of compound which produced 50% inhibition of the BChE activity (IC_{50}) was calculated by nonlinear regression of the response/concentration (log) curve, by using Prisma GraphPad software (ver. 5.01), thus plotting the initial rate values. The AChE inhibitory activity was similarly determined, by instead using a solution of AChE (0.9 U/mL in 0.1 MpH 8.0 PB), and acetylthiocholine iodide (0.05 mM) as enzyme and substrate, respectively. The inhibition data are reported as means of IC_{50} values determined at least in three independent measurements.

4.4.2. Inhibition of $A\beta_{1\text{-}40}$ aggregation

The spectrofluorimetric assays, measuring ThT fluorescence in the presence of Aβ, were done as previously described [37]. Briefly, samples of Aβ were co-incubated with test molecules in PBS at 100 μM concentration containing 2% v/v of 1,1,1,3,3,3-hexafluoro-2-propanol and the antiaggregating activities were measured after 2 h of incubation at 25 °C in 96-well black, non-binding microplates (Greiner Bio-One GmbH, Frickenhausen, Germany). Fluorimetric reads were performed in a multiplate reader Infinite M1000 Pro (Tecan, Cernusco sul Naviglio, Italy). Each concentration point was run in triplicate.

4.4.3. Cell viability and neuroprotection assay

The human neuroblastoma SH-SY5Y cell lines were purchased from American Type Culture Collection (ATCC), Rockville, MD, USA. Cells were maintained in Dulbecco's modified Eagle's medium (DMEM) supplemented with 10% of fetal bovine serum (FBS), 2 mM L-glutamine, 50 U/mL penicillin and 50 mg/mL streptomycin in a humid atmosphere of 95% air and 5% CO_2 at 37 °C, and grown to 80% of confluence. Prior the treatment, the cells were detached by mechanical agitation and plated in a 96-well plate for another 24–48h until confluence.

4.4.4. Cell viability and neuroprotection assay against NMDA or H_2O_2-induced cytotoxicity

The count of living cells was evaluated by the 3-(4,5-dimethylthiazol-2-yl)-2,5-diphenyltetrazolium bromide (MTT) assay.[35,73] In the execution, 100 μL cell suspension were plated in 96-well plates at a density of ~5000 cells/well. After 1 day of incubation at 37 °C in 5% CO_2 atmosphere, the culture medium was replaced with 100 μL of fresh medium or medium containing the test compounds at different concentrations. Untreated cells were used as positive control. After 24 h incubation, 100 μL of a 0.5% (w/v) MTT/PBS solution were added to each well and the incubation was prolonged for further 4 h. Medium was removed and replaced with 100 μL of a DMSO/ethanol (1/1 v/v) solution per well. The absorbance of the individual well was measured by a microplate reader (Wallac Victor.3, 1420 Multilabel Counter, PerkinElmer). Each compound at a single concentration was tested in triplicate, and results presented as percentage of the control value.

For the neuroprotection assay against NMDA or H_2O_2 induced stress, SH-SY5Y cells were seeded in 96-well plates at the same density used for cytotoxicity assay [35]. Cells were exposed for 24h to NMDA (250 μM) or H_2O_2 (80 μM) in reduced-serum DMEM medium at 37 °C (5% CO_2) in the absence or presence of test compounds at concentrations ranging from 1 to 20 μM. The cell viability was determined by the MTT assay. Data are presented as the mean ± SEM. The statistical comparisons were performed by one-way ANOVA followed by multiple comparison tests (Dunnett's test) using the statistical package in the GraphPad Prism software vers. 5.01.

CRediT authorship contribution statement

Francesco Samarelli: Writing – original draft, Methodology. **Rosa Purgatorio:** Writing – review & editing, Methodology. **Gianfranco Lopopolo:** Writing – review & editing, Validation. **Caterina Deruvo:** Writing – review & editing, Methodology. **Marco Catto:** Writing – review & editing, Validation, Methodology. **Michael Andresini:** Writing – review & editing, Methodology. **Antonio Carrieri:** Writing – review & editing, Validation, Software, Methodology. **Orazio Nicolotti:** Writing – review & editing, Conceptualization. **Annalisa De Palma:** Writing – review & editing, Methodology. **Daniela Valeria Miniero:** Writing – review & editing, Methodology. **Modesto de Candia:** Writing – review & editing, Writing – original draft, Validation, Supervision, Data curation, Conceptualization. **Cosimo D. Altomare:** Writing – review & editing, Supervision, Funding acquisition, Conceptualization.

Declaration of competing interest

The authors declare that they have no known competing financial interests or personal relationships that could have appeared to influence the work reported in this paper.

Data availability

The data that has been used is confidential.

Acknowledgements

R. P. was supported by funds of the Program of Regione Puglia "Research for Innovation REFIN" (POR PUGLIA FESRFSE 2014/2020). F.S was supported by "UE PO FESR 2014/2020 - Regione Puglia asse XIII"; M. d. C., R. P., M. C., and C. D. A. acknowledge the financial support of the Italian Ministry of Education, Universities and Research (PRIN, Grant 201744BN5T_004).

Appendix A. Supplementary data

Supplementary data to this article can be found online at https://doi.org/10.1016/j.ejmech.2024.116353.

References

[1] J. Cummings, Y. Zhou, G. Lee, K. Zhong, J. Fonseca, F. Cheng, Alzheimer's disease drug development pipeline: 2023, Alzheimers Dement (N Y) 9 (2023) e12385.
[2] P. Meena, V. Nemaysh, M. Khatri, A. Manral, P.M. Luthra, M. Tiwari, Synthesis, biological evaluation and molecular docking study of novel piperidine and piperazine derivatives as multi-targeted agents to treat Alzheimer's disease, Bioorg. Med. Chem. 23 (2015) 1135–1148.
[3] L.K. Pradhan, P.K. Sahoo, S. Chauhan, S.K. Das, Recent advances towards diagnosis and therapeutic fingerprinting for Alzheimer's disease, J. Mol. Neurosci. 72 (2022) 1143–1165.
[4] B. Klimova, P. Maresova, K. Kuca, Non-pharmacological approaches to the prevention and treatment of Alzheimer's disease with respect to the rising treatment costs curr, Alz. Res. 13 (2016) 1249–1258.
[5] A. Kumar, A. Singh, A. Ekavali, A review on Alzheimer's disease pathophysiology and its management: an update, Pharmacol. Rep. 67 (2015) 195–203.
[6] F. Chiti, C.M. Dobson, Protein misfolding, amyloid formation, and human disease: a summary of progress over the last decade, Annu. Rev. Biochem. 86 (2017) 27–68.
[7] J. Cummings, Anti-amyloid monoclonal antibodies are transformative treatments that redefine Alzheimer's disease therapeutics, Drugs 83 (2023) 569–576.
[8] E. Giacobini, Cholinesterase inhibitors stabilize Alzheimer's disease, Ann. NY Acad, Science 920 (2006) 321–327.
[9] W. J Geldenhuys, A.S. Darvesh, Pharmacotherapy of Alzheimer's disease: current and future trends, Expert Rev. Neurother. 15 (2015) 3–5.
[10] A. Sampietro, F.J. Pérez-Areales, P. Martínez, E.M. Arce, C. Galdeano, D. Muñoz-Torrero, Unveiling the multitarget anti-alzheimer drug discovery landscape: a bibliometric analysis, Pharmaceuticals 15 (2022) 545.
[11] M. Tonelli, M. Catto, R. Sabaté, V. Francesconi, E. Laurini, S. Pricl, L. Pisani, D. V. Miniero, G.M. Liuzzi, E. Gatta, A. Relini, R. Gavín, J.A. Del Rio, F. Sparatore, A. Carotti, Thioxanthenone-based derivatives as multitarget therapeutic leads for Alzheimer's disease, Eur. J. Med. Chem. 250 (2023) 115169.

[12] C.G. Zhan, F. Zheng, D.W. Landry, Fundamental reaction mechanism for cocaine hydrolysis in human butyrylcholinesterase, J. Am. Chem. Soc. 125 (2003) 2462–2474.
[13] P. Masson, E. Carletti, F. Nachon, Structure, activities and biomedical applications of human butyrylcholinesterase, Protein Pept, Letture 16 (2009) 1215–1224.
[14] N.H. Greig, T. Utsuki, D.K. Ingram, Y. Wang, G. Pepeu, C. Scali, Q.S. Yu, J. Mamczarz, H.W. Holloway, T. Giordano, D. Chen, K. Furukawa, K. Sambamurti, A. Brossi, D.K. Lahiri, Selective butyrylcholinesterase inhibition elevates brain acetylcholine, augments learning and lowers Alzheimer β-amyloid peptide in rodent, Proc. Natl. Acad. Sci. USA 102 (2005) 17213–17218.
[15] R. Purgatorio, M. de Candia, A. De Palma, F. De Santis, L. Pisani, F. Campagna, S. Cellamare, C.D. Altomare, M. Catto, Insights into structure-activity relationships of 3-arylhydrazonoindolin-2-one derivatives for their multitarget activity on β-amyloid aggregation and neurotoxicity, Molecules 23 (2018) 1544.
[16] C. Geula, S. Darvesh, Butyrylcholinesterase, cholinergic neurotransmission and the pathology of Alzheimer's disease, Drugs Today 40 (2004) 711–721.
[17] S. Darvesh, M.K. Cash, G.A. Reid, E. Martin, A. Mitnitski, C. Geula, Butyrylcholinesterase is associated with β-amyloid plaques in the transgenic APPSWE/PSEN1dE9 mouse model of Alzheimer disease, J. Neuropathol. Exp. Neurol. 71 (2012) 2–14.
[18] C. Galdeano, E. Viayna, P. Arroyo, A. Bidon-Chanal, J.R. Blas, D. Muñoz-Torrero, F. J. Luque, Structural determinants of the multifunctional profile of dual binding site acetylcholinesterase inhibitors as anti-Alzheimer agents, Curr. Pharmaceut. Des. 16 (2010) 2818–2836.
[19] E.G. Duysen, B. Li, S. Darvesh, O. Lockridge, Sensitivity of butyrylcholinesterase knockout mice to (-)-huperzine A and donepezil suggests humans with butyrylcholinesterase deficiency may not tolerate these Alzheimer's disease drugs and indicates butyrylcholinesterase function in neurotransmission, Toxicology 233 (2007) 60–69.
[20] T. Arendt, M.K. Bruckner, M. Lange, V. Bigl, Changes in acetylcholinesterase and butyrylcholinesterase in Alzheimer's disease resemble embryonic developmentea study of molecular forms, Neurochem. Int. 21 (1992) 381–396.
[21] Y. Furukawa-Hibi, T. Alkam, A. Nitta, A. Matsuyama, H. Mizoguchi, K. Suzuki, S. Moussaoui, Q.S. Yu, N.H. Greig, T. Nagai, K. Yamada, Butyrylcholinesterase inhibitors ameliorate cognitive dysfunction induced by amyloid-β peptide in mice, Behav. Brain Res. 225 (2011) 222–229.
[22] S. Darvesh, G.A. Reid, Reduced fibrillar β-amyloid in subcortical structures in a butyrylcholinesterase-knockout Alzheimer disease mouse model, Chem. Biol. Interact. 259 (2016) 307–312.
[23] Q. Li, H. Yang, Y. Chen, H. Sun, Recent progress in the identification of selective butyrylcholinesterase inhibitors for Alzheimer's disease, Eur. J. Med. Chem. 132 (2017) 294–309.
[24] S. Darvesh, Butyrylcholinesterase as a diagnostic and therapeutic target for alzheimer's disease, Curr. Alzheimer Res. 13 (2016) 1–5.
[25] M. Bajda, A. Wieckowska, M. Hebda, N. Guzior, C.A. Sottrifer, B. Malawska, Structure-based search for new inhibitors of cholinesterases, Int. J. Mol. Sci. 14 (2013) 5608–5632.
[26] P. Masson, M.T. Froment, C.F. Bartels, O. Lockridge, Asp70 in the peripheral anionic site of human butyrylcholinesterase, Eur. J. Biochem. 235 (1996) 36–48.
[27] Y. Nicolet, O. Lockridge, P. Masson, J.C. Fontecilla-Camps, F. Nachon, Crystal structure of human butyrylcholinesterase and of its complexes with substrate and products, J. Biol. Chem. 278 (2003) 41141–41147.
[28] S.Y. Chiou, T.T. Weng, G.Z. Lin, R.J. Lu, S.Y. Jian, G. Lin, Molecular docking of different inhibitors and activators to butyrylcholinesterase, J. Biomol. Struct. Dyn. 33 (2014) 563–572.
[29] F.H. Darras, B. Kling, J. Heilmann, M. Decker, Neuroprotective tri- and tetracyclic BChE inhibitors releasing reversible inhibitors upon carbamate transfer, ACS Med. Chem. Lett. 3 (2012) 914–919.
[30] A. Cavalli, M.L. Bolognesi, A. Minarini, M. Rosini, V. Tumiatti, M. Recanatini, C. Melchiorre, Multi-target-directed ligands to combat neurodegenerative diseases, J. Med. Chem. 51 (2008) 547–572.
[31] M.L. Bolognesi, A. Cavalli, Multitarget drug discovery and polypharmacology, ChemMedChem 11 (2016) 1190–1192.
[32] E. Simoni, S. Daniele, G. Bottegoni, D. Pizzirani, M.L. Trincavelli, L. Goldoni, G. Tarozzo, A. Reggiani, C. Martini, D. Piomelli, C. Melchiorre, M. Rosini, A. Cavalli, Combining galantamine and memantine in multitargeted, new chemical entities potentially useful in Alzheimer's disease, J. Med. Chem. 55 (2012) 9708–9721.
[33] M. Rosini, E. Simoni, A. Minarini, C. Melchiorre, Multi-target design strategies in the context of Alzheimer's disease: acetylcholinesterase inhibition and NMDA receptor antagonism as the driving forces, Neurochem. Res. 39 (2014) 1914–1923.
[34] C.B. Mishra, S. Shalini, S. Gusain, A. Prakash, J. Kumari, S. Kumari, A.K. Yadav, A. M. Lynn, M. Tiwari, Development of novel N-(6-methanesulfonyl-benzothiazol-2-yl)-3-(4-substituted-piperazin-1-yl)-propionamides with cholinesterase inhibition, anti-β-amyloid aggregation, neuroprotection and cognition enhancing properties for the therapy of Alzheimer's disease, RCS Advance 10 (2020) 17602–17619.
[35] M. de Candia, G. Zaetta, N. Denora, D. Tricarico, M. Majellaro, S. Cellamare, C. D. Altomare, New azepino[4,3-*b*]indole derivatives as nanomolar selective inhibitors of human butyrylcholinesterase showing protective effects against NMDA-induced neurotoxicity, Eur. J. Med. Chem. 125 (2017) 288–298.
[36] S.H. Lee, R. Purgatorio, F. Samarelli, M. Catto, N. Denora, M.G. Morgese, P. Tucci P, L. Trabace, H.W. Kim, H.S. Park, S.E. Kim, B.C. Lee, M. de Candia, C. D. Altomare, Radiosynthesis and whole-body distribution in mice of a 18 F-labeled azepino[4,3-b]indole-1-one derivative with multimodal activity for the treatment of Alzheimer's disease, Arch. Pharm. (Weinheim) (2023) e2300491.
[37] R. Purgatorio, M. de Candia, M. Catto, A. Carrieri, L. Pisani, A. De Palma, M. Toma, O.A. Ivanova, L.G. Voskressensky, C.D. Altomare, Investigating 1,2,3,4,5,6-hexahydroazepino[4,3-*b*]indole as scaffold of butyrylcholinesterase-selective inhibitors with additional neuroprotective activities for Alzheimer's disease, Eur. J. Med. Chem. 177 (2019) 414–424.
[38] R. Purgatorio, M. de Candia, M. Catto, M. Rullo, L. Pisani, N. Denora, A. Carrieri, A. A. Nevskaya, L.G. Voskressensky, C.D. Altomare, Evaluation of water-soluble mannich base prodrugs of 2,3,4,5-Tetrahydroazepino[4,3-b]indol-1(6H)-one as multitarget-directed agents for Alzheimer's disease, ChemMedChem 16 (2021) 589–598.
[39] J. Faist, W. Seebacher, R. Saf, R. Brun, M. Kaiser, R. Weis, New N-methylpiperazinyl derivatives of bicyclic antiprotozoal compounds, Eur. J. Med. Chem. 47 (2012) 510–519.
[40] J. Jończyk, K. Lodarski, M. Staszewski, J. Godyń, P. Zaręba, O. Soukup, J. Janockova, J. Korabecny, K. Sałat, N. Malikowska-Racia, M. Hebda, N. Szałaj, B. Filipek, K. Walczyński, B. Malawska, M. Bajda, Search for multifunctional agents against Alzheimer's disease among non-imidazole histamine H3 receptor ligands. In vitro and in vivo pharmacological evaluation and computational studies of piperazine derivatives, Bioorg. Chem. 90 (2019) 103084.
[41] a) J. Korabecny, R. Dolezal, P. Cabelova, A. Horova, E. Hruba, J. Ricny, L. Sedlacek, E. Nepovimova, K. Spilovska, M. Andrs, K. Musilek, V. Opletalova, V. Sepsova, D. Ripova, K. Kuca, 7-MEOTA-donepezil like compounds as cholinesterase inhibitors: synthesis, pharmacological evaluation, molecular modeling and QSAR studies, Eur. J. Med. Chem. 82 (2014) 426;
b) A. Więckowska, T. Wichur, J. Godyń, A. Bucki, M. Marcinkowska, A. Siwek, K. Więckowski, P. Zaręba, D. Knez, M. Głuch-Lutwin, G. Kazek, G. Latacz, K. Mika, M. Kołaczkowski, J. Korabecny, O. Soukup, M. Benkova, K. Kieć-Kononowicz, S. Gobec, B. Malawska, Novel multitarget-directed ligands aiming at symptoms and causes of Alzheimer's disease, ACS Chem. Neurosci. 9 (2018) 1195–1214.
[42] K. Ono, K. Hasegawa, H. Naiki, M. Yamada, Curcumin has potent anti-amyloidogenic effects for Alzheimer's beta-amyloid fibrils in vitro, J. Neurosci. Res. 75 (2004) 742–750.
[43] W. Liu, H. Wang, X. Li, Y. Xu, J. Zhang, W. Wang, Q. Gong, X. Qiu, J. Zhu, F. Mao, H. Zhang, J. Li, Design, synthesis and evaluation of vilazodone-tacrine hybrids as multitarget-directed ligands against depression with cognitive impairment, Bioorg. Med. Chem. 26 (2018) 3117–3125.
[44] M. Shaquiquzzaman, G. Verma, A. Marella, M. Akhter, W. Akhtar, M.F. Khan, S. Tasneem, M.M. Alam, Piperazine scaffold: a remarkable tool in generation of diverse pharmacological agents, Eur. J. Med. Chem. 102 (2015) 487–529.
[45] U.D. Ozkay, O.D. Can, Y. Ozkay, Y. Oztürk, Effect of benzothiazole/piperazine derivatives on intracerebroventricular streptozotocin-induced cognitive deficits, Pharmacol. Rep. 64 (2012) 834–847.
[46] G.L. Ellman, K.D. Courtney, V. Andres, R.M. Feather-Stone, A new and rapid colorimetric determination of acetylcholinesterase activity, Biochem. Pharmacol. 7 (1961) 88–95.
[47] R. Zhang, F. Monsma, Binding kinetics and mechanism of action: toward the discovery and development of better and best in class drugs, Expet Opin. Drug Discov. 5 (2010) 1023–1029.
[48] G. Dahl, T. Akerud, Pharmacokinetics and the drug-target residence time concept, Drug Discov. Today 15–16 (2013) 697–707.
[49] D.N. Patil, S.A. Patil, S. Sistla, J.P. Jadhav, Comparative biophysical characterization: a screening tool for acetylcholinesterase inhibitors, PLoS One 14 (2019) e0215291.
[50] E. Fabini, A. Tramarin, M. Bartolini, Combination of human acetylcholinesterase and serum albumin sensing surfaces as highly informative analytical tool for inhibitor screening, J. Pharm. Biomed. Anal. 155 (2018) 177–184.
[51] O. Yildiz, E. Bodur, A.N. Cokuğraş, N. Ozer, Partial purification and characterization of soluble isoform of butyrylcholinesterase from rat intestine, Protein J. 23 (2004) 143–151.
[52] G. Vauquelin, Effects of target binding kinetics on in vivo drug efficacy: k_{off} , k_{on} and rebinding, Br. J. Pharmacol. 173 (2016) 2319–2334.
[53] Y. Zhou, Y. Fu, W. Yin, J. Li, W. Wang, F. Bai, S. Xu, Q. Gong, T. Peng, Y. Hong, D. Zhang, D. Zhang, Q. Liu, Y. Xu, H.E. Xu, H. Zhang, H. Jiang, H. Liu, Kinetics-driven drug design strategy for next-generation acetylcholinesterase inhibitors to clinical candidate, J. Med. Chem. 64 (2021) 1844–1855.
[54] M. Rossi, M. Freschi, L. De Camargo Nascente, A. Salerno, S. De Melo Viana Teixeira, F. Nachon, F. Chantegreil, O. Soukup, L. Prchal, M. Malaguti, C. Bergamini, M. Bartolini, C. Angeloni, S. Hrelia, L.A. Soares Romeiro, M. L. Bolognesi, Sustainable drug discovery of multi-target-directed ligands for alzheimer's disease, J. Med. Chem. 64 (2021) 4972–4990.
[55] N. Di Marzo, E. Chisci, R. Giovannoni, The role of hydrogen peroxide in redox-dependent signaling: homeostatic and pathological responses in mammalian cells, Cells 7 (2018) 156.
[56] B.D. Belviso, R. Caliandro, M. de Candia, G. Zaetta, G. Lopopolo, F. Incampo, M. Colucci, C.D. Altomare, How a β-D-glucoside side chain enhances binding affinity to thrombin of inhibitors bearing 2-chlorothiophene as P1 moiety: crystallography, fragment deconstruction study, and evaluation of antithrombotic properties, J. Med. Chem. 57 (2014) 8563–8575.
[57] Swiss Institute of Bioinformatics. http://www.swissadme.ch/index.php (accessed 15 March 2024).
[58] A. Daina, V. Zoete, A BOILED-egg to predict gastrointestinal absorption and brain penetration of small molecules, ChemMedChem 11 (2016) 1117–1121.
[59] F. Cheng, W. Li, Y. Zhou, J. Shen, Z. Wu, G. Liu, P.W. Lee, Y. Tang, AdmetSAR: a comprehensive source and free tool for assessment of chemical ADMET properties, J. Chem. Inf. Model. 52 (2012) 3099–3105.

[60] N.M. O'Boyle, M. Banck, C.A. James, C. Morley, T. Vandermeersch, G. R. Hutchison, Open Babel: an Open Chemical Toolbox, 2011.
[61] QUACPAC Package, Vers. 2.1.0.4, OpenEye Scientific Software, Santa Fe, NM..
[62] S.K. Burley, H.M. Berman, C. Bhikadiya, C. Bi, L. Chen, L. Di Costanzo, C. Christie, J.M. Duarte, S. Dutta, Z. Feng, S. Ghosh, D.S. Goodsell, R.K. Green, V. Guranovic, D. Guzenko, B.P. Hudson, Y. Liang, R. Lowe, E. Peisach, I. Periskova, C. Randle, A. Rose, M. Sekharan, C. Shao, Y.P. Tao, Y. Valasatava, M. Voigt, J. Westbrook, J. Young, C. Zardecki, M. Zhuravleva, G. Kurisu, H. Nakamura, Y. Kengaku, H. Cho, J. Sato, J.Y. Kim, Y. Ikegawa, A. Nakagawa, R. Yamashita, T. Kudou, G.J. Bekker, H. Suzuki, T. Iwata, M. Yokochi, N. Kobayashi, T. Fujiwara, S. Velankar, G. J. Kleywegt, S. Anyango, D.R. Armstrong, J.M. Berrisford, M.J. Conroy, J.M. Dana, M. Deshpande, P. Gane, R. Gáborová, D. Gupta, A. Gutmanas, J. Koča, L. Mak, S. Mir, A. Mukhopadhyay, N. Nadzirin, S. Nair, A. Patwardhan, T. Paysan-Lafosse, L. Pravda, O. Salih, D. Sehnal, M. Varadi, R. Vařeková, J.L. Markley, J.C. Hoch, P. R. Romero, K. Baskaran, D. Maziuk, E.L. Ulrich, J.R. Wedell, H. Yao, M. Livny, Y. E. Ioannidis, Protein Data Bank: the single global archive for 3D macromolecular structure data, Nucleic Acids Res. 47 (2019) D520–D528.
[63] Schrödinger Release 2023-1: BioLuminate, Schrödinger, LLC, New York, NY, 2023.
[64] W.D. Cornell, P. Cieplak, C.I. Bayly, I.R. Gould, K.M. Merz, D.M. Ferguson, D. C. Spellmeyer, T. Fox, J.W. Caldwell, P.A. Kollman, A second generation force field for the simulation of proteins, nucleic acids, and organic molecules, J. Am. Chem. Soc. 117 (1995) 5179–5197.
[65] G.M. Morris, D.S. Goodsell, R.S. Halliday, R. Huey, W.E. Hart, R.K. Belew, A. J. Olson, Automated docking using a lamarckian genetic algorithm and an empirical binding free energy function, J. Comput. Chem. 19 (1999) 1639–1662.
[66] L. El Khoury, D. Santos-Martins, S. Sasmal, J. Eberhardt, G. Bianco, F.A. Ambrosio, L. Solis-Vasquez, A. Koch, S. Forli, D.L. Mobley, Comparison of affinity ranking using AutoDock-GPU and MM-GBSA scores for BACE-1 inhibitors in the D3R Grand Challenge 4, J. Comput. Aided Mol. Des. 33 (2019) 1011–1020.
[67] S. Forli, A.J. Olson, A force field with discrete displaceable waters and desolvation entropy for hydrated ligand docking, J. Med. Chem. 55 (2012) 623–638.
[68] A. Carocci, A. Barbarossa, R. Leuci, A. Carrieri, L. Brunetti, A. Laghezza, M. Catto, F. Limongelli, S. Chaves, P. Tortorella, C.D. Altomare, M.A. Santos, F. Loiodice, L. Piemontese, Novel phenothiazine/donepezil-like hybrids endowed with antioxidant activity for a multi-target approach to the therapy of alzheimer's disease, Antioxidants 11 (2022) 1631.
[69] K. Czarnota-Łydka, S. Sudoł-Tałaj, K. Kucwaj-Brysz, R. Kurczab, G. Satała, M. de Candia, F. Samarelli, C.D. Altomare, A. Carocci, A. Barbarossa, E. Żesławska, M. Głuch-Lutwin, B. Mordyl, M. Kubacka, N. Wilczyńska-Zawal, M. Jastrzębska-Więsek, A. Partyka, N. Khan, M. Więcek, W. Nitek, E. Honkisz-Orzechowska, G. Latacz, A. Wesołowska, A. Carrieri, J. Handzlik J, Synthesis, computational and experimental pharmacological studies for (thio)ether-triazine 5-HT6R ligands with noticeable action on AChE/BChE and chalcogen-dependent intrinsic activity in search for new class of drugs against Alzheimer's disease, Eur. J. Med. Chem. 259 (2023) 115695.
[70] ROCS Package, Vers. 3.4.0.4, OpenEye Scientific Software, Santa Fe, NM..
[71] R. Purgatorio, N. Gambacorta, M. de Candia, M. Catto, M. Rullo, L. Pisani, O. Nicolotti, C.D. Altomare, First-in-Class isonipecotamide-based thrombin and cholinesterase dual inhibitors with potential for alzheimer disease, Molecules 26 (2021) 5208.
[72] R. Purgatorio, N. Gambacorta, F. Samarelli, G. Lopopolo, M. de Candia, M. Catto, O. Nicolotti, C.D. Altomare, Assessing the role of a malonamide linker in the design of potent dual inhibitors of factor Xa and cholinesterases, Molecules 27 (2022) 4269.
[73] M. Rullo, M. Cipolloni, M. Catto, C. Colliva, D.V. Miniero, T. Latronico, M. de Candia, T. Benicchi, A. Linusson, N. Giacchè, C.D. Altomare, L. Pisani, Probing fluorinated motifs onto dual AChE-MAO B inhibitors: rational design, synthesis, biological evaluation, and early-ADME studies, J. Med. Chem. 65 (2022) 3962–3977.